University ”POLITEHNICA” of Bucharest

Doctoral School of Applied Sciences

Exact Sciences, Physics Departament

**Georgiana-Diana CHIOIBAȘU**

# Medical devices of Titanium alloys obtained by laser additive manufacturing techniques

# Dispozitive medicale din aliaje de Titan obținute prin tehnici laser de fabricație aditivă

Doctoral committee:

| | | |
|---|---|---|
| Chair of the committee | **Prof. Univ. Dr. Cristina STAN** | University POLITEHNICA of Bucharest |
| Supervisor | **Prof. Univ. Dr. Niculae PUȘCAȘ** | University POLITEHNICA of Bucharest |
| Member | **Dr. Marian ZAMFIRESCU** | National Institute for Laser, Plasma and Radiation Physics |
| Member | **Prof. Univ. Dr. Cristina MOHORA** | University POLITEHNICA of Bucharest |
| Member | **Dr. Andrei POPESCU** | National Institute for Laser, Plasma and Radiation Physics |

Bucharest
2021

# TABLE OF CONTENTS

# 1. INTRODUCTION AND STATE OF THE ART

Laser material processing has been intensely studied since 1960s, when Theodore Maiman built the first laser source with ruby active medium emitting in deep red (694.3 nm wavelength) [1], [2]. This laser system was used in aircraft industry for drilling cooling holes in the turbine blades of an engine to prevent thermal damage. Starting from this application, laser material processing was widely extended to many industrial applications, such as laser cutting [3]–[10], laser welding [11]–[20], laser ablation [21]–[26], laser marking [27]–[31], pulsed laser deposition (PLD) [32]–[36] or laser additive manufacturing (LAM) [17], [37]–[40].

Our research group fields of expertise covers topics like laser welding, pulsed laser deposition, ultra-short laser ablation, laser direct writing and laser additive manufacturing.

Additive manufacturing (AM) is the center of this study, so we will narrow the list to this topic. AM is an emergent technique for fabrication of three-dimensional (3D) parts [41]–[46] with near-net shape directly from a CAD model by adding material in a layer by layer manner [47]–[49]. According to ISO 17296-2:2015 (Additive manufacturing, general principles, overview of process categories, and feedstock) [50] there are seven AM categories, as follows: VAT photopolymerization [51]–[53], binder jetting [54]–[57], material extrusion [58]–[62], material jetting [66]–[69], sheet lamination [67]–[70], powder bed fusion (PBF) [74]–[79] and direct energy deposition (DED) [77]–[82]. The last two processes are the most common when dealing with metallic materials [47] and they will be amply treated in this thesis.

For both methods, PBF and DED, the design process is essential. By using a proper dedicated software that permits topological optimization, material can be eliminated from the areas with low tensions, obtaining lighter parts with up to 33%, but withstanding the same mechanical properties as the conventional design [83].

After part-producing step, a post-processing phase is required most of the times. First of all, the components have to be removed from the substrate. Independent of the material type or method, the parts obtained by AM processes are generally characterized by a rough surface, due to partial melting of the powder particles, metal flow, as well as the layer by layer pattern [84]. The surface roughness values in the range of Ra 4 to Ra 100 have been reported in the case of LMD parts, while for SLM components, it can be between Ra 5 to Ra 10 [85], [86]. Table 1.1 highlights the differences between various features of PBF and DED [87].

**Table 1.1 Comparison between various features of interest for PBF and DED.**

| Feature | DED | PBF |
|---|---|---|
| Raw materials | Powder, wire | Powder |
| Heat source | Laser | Laser, electron beam |
| Technology | Powder is sprayed through a nozzle and melted by a laser beam | Beam transfers heat that melts a powder bed |

| | | |
|---|---|---|
| Typical materials | Metals, ceramics | Metals, ceramics, polymers |
| Limitations by direction/axis | No | Yes |
| Resolution | Low | High |
| Versatility | High: used for coating, parts manufacturing, and in situ alloying | Low: limited to parts production |
| Parts size | Usually large scale objects | Usually small scale objects |
| The possibility of parts repair | Yes | No |
| Structural and compositional in situ modifications | Yes: easy to produce multi-structures and parts with compositional gradient, allows for in situ alloying | No: limited to one type of powder/cycle |
| Mesh structures | No | Yes |
| Post-processing requirements | Yes | Yes |
| Costs | High: high power laser sources and robots required | Lower: more compact machines, easy to implement in industry |
| Application in the biomedical field | Currently very low | Quite advanced: e.g., implemented in dental cabinets for the manufacturing of personalized dental prostheses |

In Romania, additive manufacturing of metals is inclined towards PBF technology, especially SLM [88]–[91] using metallic powders for many different applications such as biomedical (cranial [92], [93], maxillofacial bone [94] and dental [95], [96] personalized implants, lattice structure [97] or dental tools [98]), automotive [99] and aerospace [100]. However, PBF it`s also a suitable method for 3D printing of parts starting from polyamide [72], [101] or ceramics [102], [103] powders. In the scientific literature, this AM method is known as Fused Deposit Modelling (FDM) [104], [105]. In our country, it`s affordable price and the possibility to print large scale components propelled it as one of the most researched AM techniques. Recently, using FDM, medical face shields (necessary in the fight against Covid-19 pandemic crisis) [106] were produced by biodegradable thermoplastic polymer with a lighter mass, lower cost and faster fabrication time as compared to conventional techniques. To the opposite pole, DED it is not so well expended in Romania, the high cost being a probable cause, due to the necessity of using high power laser sources and robots. Based on the public reported

information, the only DED equipment in Romania it is the one in LaMP (Laser Materials Processing Laboratory) in CETAL (Center for Advanced Laser Technologies) in Magurele. However, because this technique opens a wide area of applications and it is still far from reaching the industrial maturity, there is a possibility that such equipment's may exist in large companies in Romania, but not yet be commercially exploited. We acknowledge two examples of such cases, i.e. the existence of a hybrid AM machine designed for rapid prototyping of turbocharger components in a company named Compa [107] and a DED pilot machine acquired by the company S.C. Optoelectronica 2001 S.A, with deposition technology provided by our Laboratory, in the framework of a knowledge transfer project.

The thesis *"Medical devices of titanium alloys obtained by laser additive manufacturing techniques*" presents our studies on fabrication of medical devices by 3D printing techniques. In this study, we intended to improve the resolution of parts manufactured by LMD through design and process optimization (laser power, velocity, powder debit, scanning strategy), as well as to fabricate different devices for several medical applications. The samples obtained in this thesis were subjected to *in vitro* and *in vivo* testing, in order to demonstrate the biocompatibility and functionality of the obtained parts.

Implantable medical devices represent a reasonable application target for 3D printing techniques due to the requirement for implants with custom-made shapes and dimensions, imposed by features of the impaired tissue, envisaged to be treated, reinforced or substituted [108]–[111].

Following this introduction chapter, the second chapter introduces a succinct theoretical background that comprises analytical models of energy and temperature distribution in additive manufacturing of metallic materials. The first section highlights a series of equations that matches to a genuine LMD system. Energy distribution and melt pool temperature can be determined starting from the process parameters and powder material properties. Preliminary assumptions were drawn for a simplified analytical model which takes under consideration the energy above and into the molten pool. Multi-layers and single track temperature distribution are considered in order to establish the scanning strategy and the height of the build.

The third chapter presents the methods and materials that were used for additive manufacturing processes. It contains specifics of processing parameters influence, experimental setup, types of laser sources and samples characterization. We start with general considerations of the laser additive manufacturing of metallic materials by presenting the type of lasers used for the experiments presented in this thesis and we describe the programming procedure. The principle of LMD technique is detailed together with the CAM interface software used to program the scanning strategies, in order to obtain parts according to the technical drawings. We present the optimal process parameters for manufacturing of Ti parts without internal defects and the calibration curve developed to get a congruent match between CAD drawings and the manufactured part's dimensions

In the fourth chapter, we present in detail the fabrication process of 3D printed samples. The section is structured in four subchapters, each containing a research study on this thematic.

The first subchapter describes a quality improvement of Ti6Al4V parts manufactured by LMD. We eliminated the internal defects of the structures by tuning the experimental parameters of the LMD process based on data provided by an X-Ray Computed Tomography system, which proved to be an exceptional tool to assess defects in the bulk material.

The second subsection comprises the fabrication of orthopedic bone plates of Ti6Al4V by LMD. By optimizing the process parameters and scanning strategies we obtained dense, flawless and uniform compositional distribution depositions. The design of the trajectory followed by the laser beam proved to be essential for obtaining adequate shapes. The incipient 3D prints were cut, drilled and polished to get the final implant. In vitro tests with osteosarcoma cells, more precisely, MTS tests have shown that cells proliferate, which mean that the materials printed by LMD are biocompatible.

In the third subchapter, we present a research in which 3D printed medical devices made by LMD were coated with biological-derived hydroxyapatite doped with lithium carbonate (Li-C) and phosphate (Li-P) and tested in vitro. The inferred detachment force values of the functionalized Ti implants were ~2 times higher than those registered for the uncoated ones. The extraction test results indicated improved bonding strength values (~5 times higher) of the functionalized Ti implants as compared to the same structures, but corresponding to an implantation time period of 4 weeks.

In the fourth subsection we describe the manufacturing by SLM of metallic prostheses starting from Ti6Al4V metallic powders, by comparing the results with those obtained by LMD. We also optimized irradiation parameters in order to obtain shapes without defects, such as pores or cracks, with uniform elemental distribution in the bulk. Cranial prostheses produced by 3D printing were coated by radio-frequency magnetron sputtering with a very thin layer of hydroxyapatite of animal origin. The material was bioactive, osteoblast cells proliferating between 1-7 days at a higher rate as compared to bare Ti controls.

The last chapter of this thesis is dedicated to a short discussion of the presented results, conclusions and future planned work.

# 2. THEORETICAL BACKGROUND FOR ADDITIVE MANUFACTURING OF METALS

This chapter offers a theoretical background for a better understanding of the additive manufacturing process in case of metals [112]. Analytical models used in practice for predictions of surface temperature and for tuning of the most important parameters are provided, while supplemental bibliographic references are given, if the reader desires to search the topic more in depth.

The first section contains information concerning energy distribution in LMD process. The model described in this section provides essential information about the energy generated by the laser source above the molten pool, energy absorption by the molten pool and temperature distribution during the process. The laser-powder interaction, the effect of the heated powder and the wasted powder are taken into consideration in order to round the analytical modeling. The equations are developed with the aim to be applied on a genuine LMD process [113] using metallic powders [114] and proved to offer reliable outcomes by the experimental data.

In the current study, the energy distribution in the laser cross-section of the beam has been considered as top-hat. It ensures a uniform energy distribution in the irradiated area. Additionally, the top-hat laser processing leads to better control of surface quality and structuring of depositions as compared to non-uniform energy distributions spots such as Gaussian beams.

A three-jet powder stream, generated by a nozzle (Trumpf, Ditzingen, Germany) mounted on a robot (KR30HA, Kuka, Augsburg, Germany) equipped with LMD optics, was recorded via high-speed imaging camera (AX100, Photron, Tokyo, Japan). 1000 frames per second and shutter speed equal to 1/5000 s, were used to acquire the powder flow shape. The KUKA robot translates a top-hat ytterbium-doped yttrium aluminium garnet (Yb: YAG) laser beam with a wavelength equal to 1030 nm. Figure 2.1a shows an optical image for the powder stream distribution using a three-jet powder nozzle, which is used for the comparison between (powder stream) analytical and experimental results. The details regarding the parameters, including the intersection point of the three sub-nozzles and width of the powder stream in the Gaussian form, were determined via “Image J” software (1.53a, National Institute of Health and the Laboratory for Optical and Computational Instrumentation, Wisconsin, USA), as presented in Figure 2.1b.

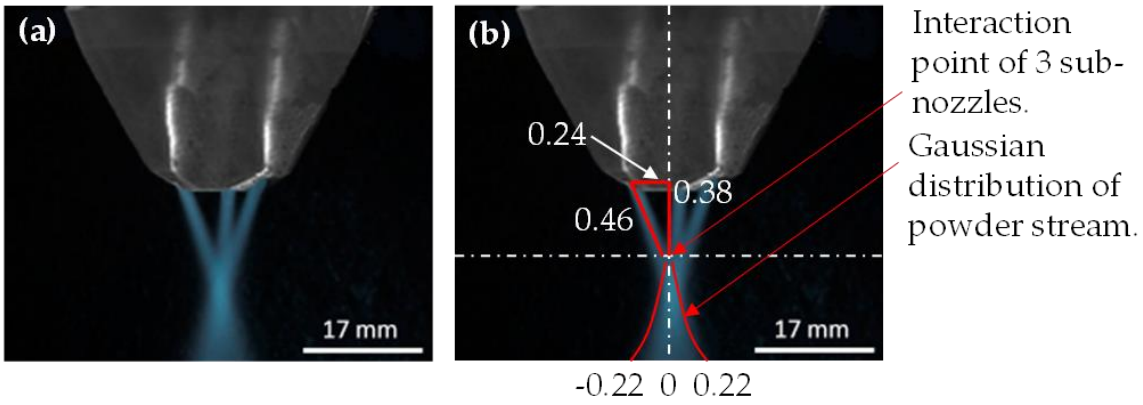


**Figure 2.1.** A three-jet powder stream distribution (a) experimental image and (b) image processed via "Image J" software; all units are in millimeter (mm) [112].

Figure 2.2 illustrates a comparison between the experimental (see Figure 2.1) and computational results. Besides, the influence of the focal point position on the powder stream distribution was analyzed. A close correlation can be observed between the experimental and simulation results (Figure 2.2). The results indicate that the powder stream follows the Gaussian distribution at the focal plane, focal plane + 1 mm distance, and focal plane + 2 mm distance. However, the peak point of the Gaussian curve decreases while the standard deviation increases, resulting in an extended powder spread on the substrate. At the focal plane + 2.5 mm distance, the powder stream shifts from the Gaussian to the Transition stream, while at focus plane + 3 mm distance, the powder flow no longer remains in the Transition state. Instead, an Annular powder stream can be observed in Figure 2.2. Hence, the powder flow can be divided into three different regimes: (a) Gaussian stream, (b) Transition stream, and (c) Annular stream. This study displays a good correlation with the experimental findings given in [115].

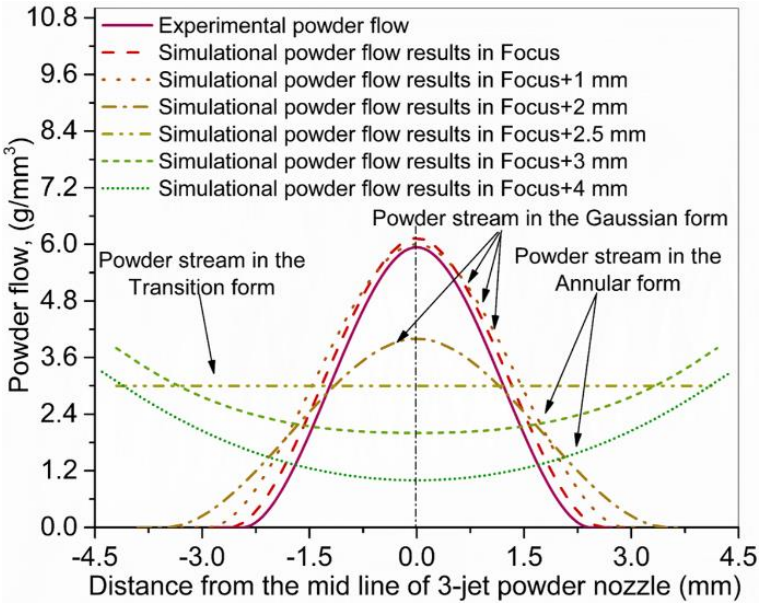


**Figure 2.2.** Comparison of Ti6Al4V titanium alloy powder flow experimental and simulation results: Influence of the focal point position on powder stream distribution regimes [112].

The powder particles undergo two types of heating: (a) inflight, and (b) within the melt-pool. The inflight heating of the powder particles can be directly controlled by the laser-powder particles' interaction time required to initiate the vaporization, while the heating of powder particles within the melt-pool can be indirectly monitored by the laser-substrate interaction time via scanning speed.

# 3. MATERIALS AND METHODS

## 3.1 LASER MELTING DEPOSITION

LMD is an additive manufacturing method used mostly for metals and metal matrix composites. It implies to blow a metallic powder into a molten pool created by a laser beam on a substrate. By melting of the powder followed by solidification, a first layer is deposited. Next, the laser beam and the powder nozzle are translated upwards with a predetermined value, and a new layer of deposited material is added on the top of the first layer. By repeating this step, a new part is 3D printed. The process is suitable for the fabrication of composite materials [116] or compositional graded materials [117] as it can concurrently feed multiple types of powders via multi-hopers. Additionally, LMD is ideal to repair parts with minimum waste [118], to add new elements on casted parts, to build full components or to fabricate heterogeneous components. Usually the components manufactured by LMD have comparable or even improved mechanical properties compared to original pieces conventionally obtained by casting [119].

The experimental set-up from our laboratory is comprises of a 3 kW Yb:YAG laser source (TruDisk 3001) emitting in continuous wave with wavelength $\lambda$=1030 nm (fig.3.1.a) connected by optical fiber to a deposition optics. The optics are mounted on a robotic arm (TruLaser Robot 5020) with 8 degrees of freedom (fig.3.1.b) using an electro-magnetic plate. The metallic powder is transported from the container storage of the powder feeder to the work-piece through hoses with diameter up to Ø5 mm (fig.3.1.c). The deposition line is equipped with a nozzle (fig.3.1.d) which ensures a uniform powder distribution, independent of the process motion. We have two types of nozzles available in the laboratory: i) a three beam nozzle (16 mm-nozzle distance standoff, 4 mm powder focus diameter and up to 5 kW permissible laser power) which ensures high deposition rates and ii) a coaxial nozzle (7 mm-nozzle distance standoff, 1 mm powder focus diameter and up to 1 kW permissible laser power) for a higher resolution of the tracks and dedicated to intricate structures printing. The laser beam is guided and focused on the workpiece trough the focusing optics, while the powder stream is blown into the laser spot. The process is assisted by shroud gas ($N_2$ or Ar) which has the role to protect the new coating from oxidation.

Before experiments, all types of metallic powders used in the following subsections were analyzed by Computer Tomography (CT) to reveal if there were voids inside the particles at large scale, but also to determine the distribution of powder particles by volume. The results are presented in subsection 4.1.

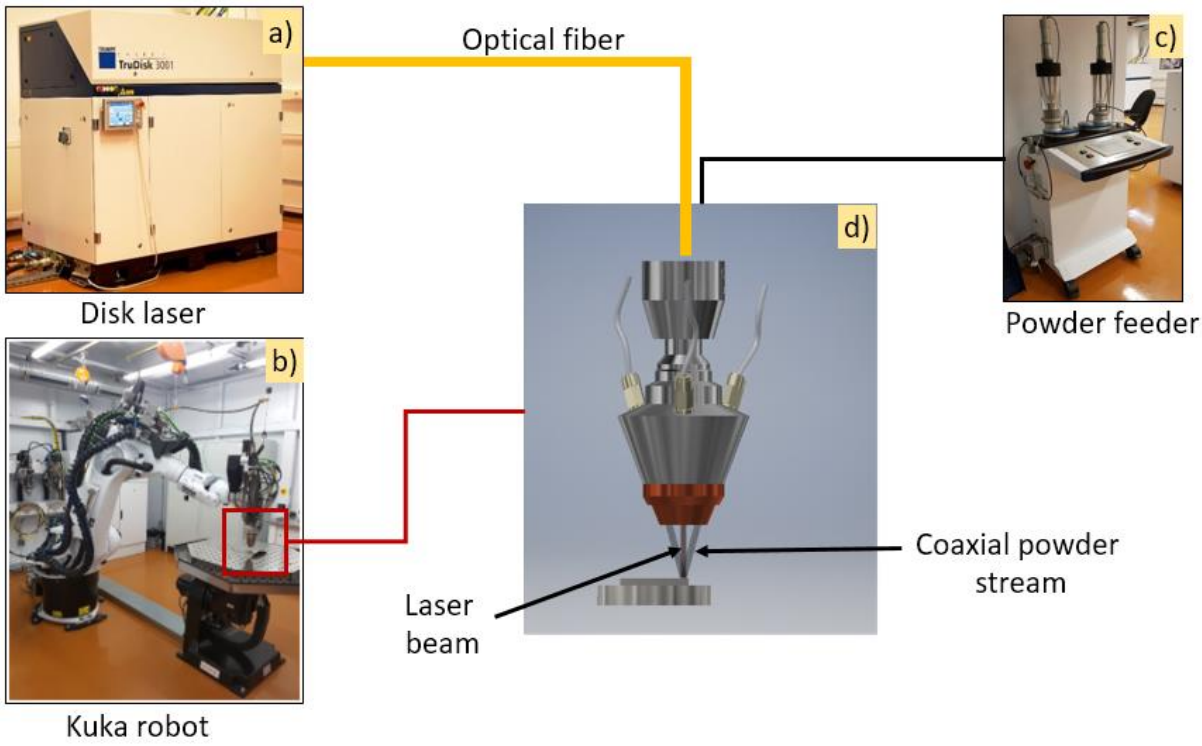


**Figure 3.1** Laser Melting Deposition experimental set-up composed of (a) laser system, (b) robot arm, (c) powder feeder, (d) focusing system of the laser beam and powder jet

Using the LMD method, we fabricated three types of medical devices: implant fasteners, bone and spinal plates. The medical devices were manufactured using the experimental setup described in the above section. The products were fabricated on a 10 mm thick Ti plate using Ti6Al4V micronic powders purchased from Carpenter Additive (Widnes, UK) with the particle dimensions in the range of 45-109 µm.

Dense deposition tracks without defects were obtained using 700 W laser power, 0.015 m/s velocity, 3 gr/min powder flow and 10 slpm Ar-He carrier gas.

## 3.2 SELECTIVE LASER MELTING

Selective Laser Melting (SLM) is a powder bed AM method, also known as direct metal laser melting or laser powder bed fusion in which the components are manufactured in a layer by layer manner. A 3D CAD model is generated using an engineering software and then is imported in the machine computer, where it is virtually sliced in 2D thin layers. The parts are manufactured on a thick substrate which is fixed on a heated platform (40-80ºC) to reduce internal stress and ensure a good bonding starting from the first layer. The SLM machine is equipped with a laser source (Yb fiber laser, $\lambda$= 1060-1100 nm and nominal power up to 200 W), a high-speed scanner optics containing precision galvanometer scanners (exposure area 250 mm x 250 mm and exposure speed up to 7000 mm/s). The laser beam focused by an F-theta objective (diameter of the laser beam 100 -500 µm and focal length 410 mm) is melting the powders spread all over the substrate. Then, the build plate is lowered with an equal step as the height of the layer created by the laser scanning and the top of the part is covered by a new layer of powder by the leveling system. This step is repeated until the shape is generated in it's entirety. The manufacturing process is conducted under controlled Ar atmosphere. All the

components described above are part of an integrated SLM machine, model M270 (Eos GmbH, Germany). A schematic of SLM working principle is presented in the figure 3.2.

***Cranial implants produced by SLM***

The technical design of the cranial meshes is presented in Appendix 3. For the part fabrication, we used Ti6Al4V powder with particles diameters in the range of 10 to 30 µm. The optimum parameters for melting the powder were 90 W laser power with 0.45 m/s scanning speed under 4 bar Ar atmosphere and the laser beam was focused at 100 µm on the bed powder. Once the 3D printing process was completed, the part was removed from the substrate using an electro - erosion cutting machine Robofil 6030 (Charmilles Technologies, Switzerland). A detailed material about the post-processing steps can be found in subsection 4.3.

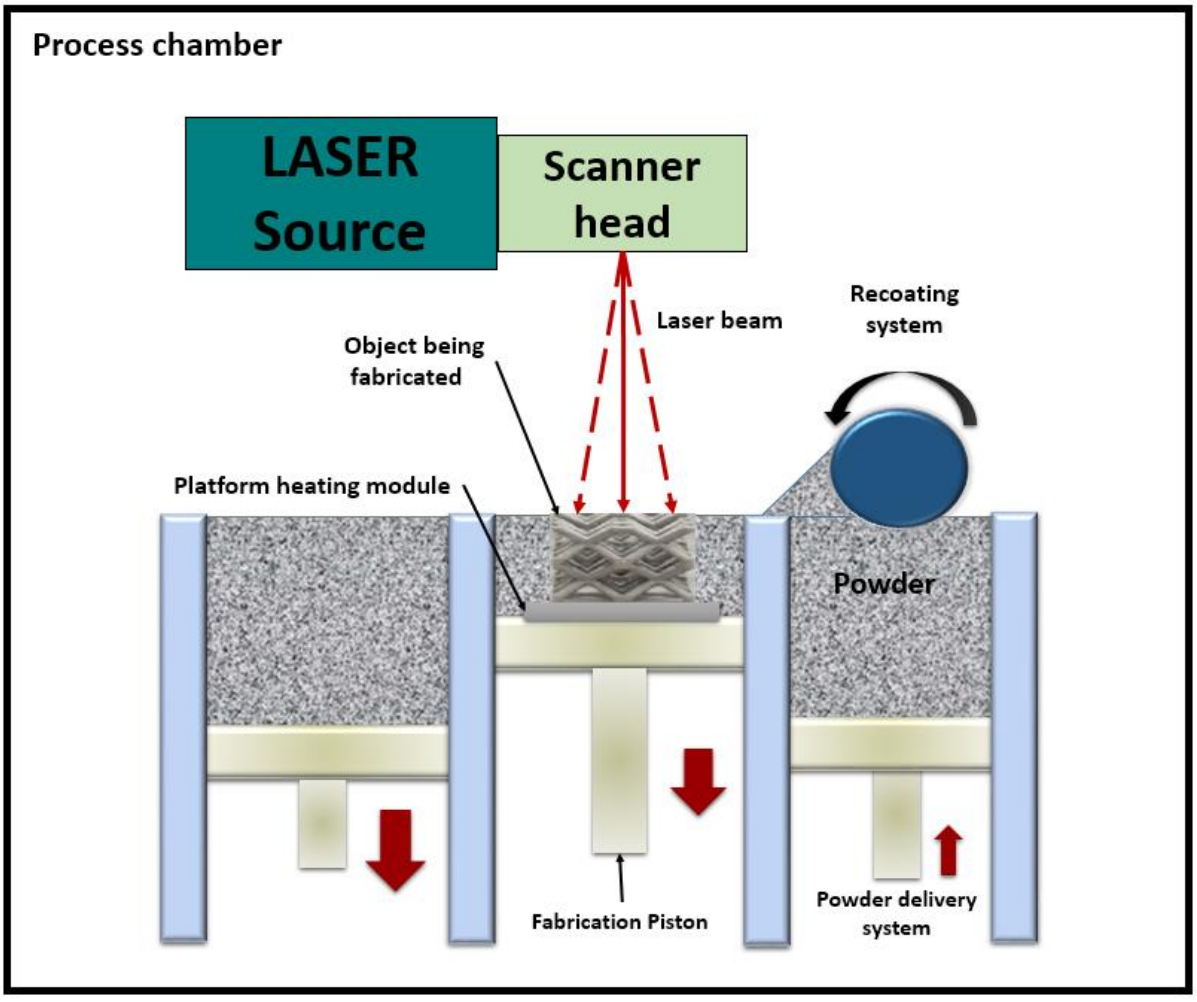


**Figure 3.2** Selective Laser Melting working principle

## 3.3 PHYSICO-CHEMICAL CHARACTERIZATIONS

### *3.3.1 Metallographic characterization and micro-hardness*

The metallographic characterization is the first analysis in the quality assessment process. This destructive analysis is required to establish the optimum set of parameters in order to

obtain a required metallographic structure and to eliminate defects in the bulk. The specimens are cut in small pieces, embedded in resin, grinded and polished mirror alike.

In order to reveal the metallographic structure, the polished surfaces were chemically etched with a Kroll Reagent. The samples treated with the chemical reagent were studied by optical microscopy using a DM4000 B LED instrument (Leica, Wetzlar, Germany). In order to evidence the compactness of the LMD synthesized material, samples unexposed to the reagent were also studied by optical microscopy.

The hardness of the bulk structures was determined by a Vickers microdurimeter, model FM-700 (Future Tech, Holbrook, USA), using a load of $5 \times 10^{-2}$ N [120].

### *3.3.2 Scanning electron microscopy*

The microstructures of the results samples were analyzed by scanning electron microscopy (SEM), using an EVO 50XVP (Carl Zeiss, Oberkochen, Germany) instrument.

The compositions of the source powders, LMD and SLM samples were assessed by energy dispersive X-ray spectroscopy (EDXS) by means of a 133 eV XFlash 4010 (Bruker AXS, Karlsruhe, Germany) attached to the SEM microscope. The EDXS analyses were performed in four different large ($533 \times 360$ μm$^2$) regions of the specimens in order to average over possible compositional non-homogeneities. Mean ± standard deviation values were computed. Further statistical analyses were carried out using the unpaired Student's *t*-test, with differences being considered significant at a probability value ($p$) < 0.05. The surface homogeneity of the LMD sample was probed by EDXS elemental mapping [120].

X-ray diffraction (XRD) investigations were performed with a D8 Advance (Bruker AXS Karlsruhe, Germany) apparatus using $CuK_\alpha$ ($\lambda = 1.5418$ Å) radiation and a rapid LynxEye™ detector. The samples were scanned in symmetric geometry (θ–θ), in the 2θ angular range 25°–75°, using a step of 0.04° and time per step of 2 s. The XRD analysis aimed to provide qualitative and quantitative information about the crystalline phases. The XRD data processing was performed using the TOPAS® (Bruker, Karlsruhe, Germany) software. A corundum reference sample (NIST SRM 1976) was used to verify the alignment of the instrument and to model the instrumental line profiles [120].

### *3.3.3 In vitro testing*

The printed samples were cut in $3 \times 6$ mm$^2$ coupons for in vitro testing. Before the biological assays, all the mirror-polished coupons were steam-sterilized at 121 °C for 30 min, using an AES-8 autoclave (Raypa, Barcelona, Spain) [120].

### *3.3.4 Cell culture*

Human osteosarcoma cells (SaOs2) were cultured in McCoy's 5A medium (Gibco, Waltham, USA) supplemented with 15% fetal bovine serum (FBS) (Gibco, Waltham, MA, USA) and 1% penicillin (10,000 U/mL)-streptomycin (10000 μg/mL) (PEN-STREP) (Gibco, Waltham, MA, USA). The cells were split at passage P19 and seeded on the coupons placed in 24-well tissue-culture test plates (TPP Techno Plastic Products AG, Trasadingen, Switzerland) at a density of 15000 cells/sample. They were cultured in a 5% $CO_2$ humid atmosphere at 37 °C for 1, 3, and 7 days. Glass coverslip (CS) of 12 mm diameter was used as an experimental

control. The cells cultivated on CS were routinely visualized by using a Leica DMi1 (Leica Microsystems, Wetzlar, Germany) inverted phase contrast microscope [120].

### *3.3.5 MTS assay*

Cell proliferation was investigated using a CellTiter 96 aqueous solution cell viability kit from Promega (Madison, WI, USA). The assay is based on the use of a tetrazolium compound (3-(4,5-dimethylthiazol-2-yl)-5-(3-carboxymethoxyphenyl)-2-(4-sulfophenyl)-2*H*-tetrazolium, inner salt—MTS) that is chemically reduced by viable cells into formazan, which is soluble in the tissue culture medium. Since the production of formazan is proportional to the number of living cells, the intensity of the produced color can be used as an indicator of cell proliferation.

### *3.3.6 Immunofluorescence microscopy*

Cells grown on all samples were examined by means of fluorescence imaging. After 24 h and 72 h of culture, SaOs2 cells were fixed with 4% paraformaldehyde at room temperature and kept in phosphate-buffered saline (PBS) at 4 °C before labeling. The fixed cells were then permeabilized with 0.2% TritonX-100 and blocked in 0.5% bovine serum albumin. In order to visualize the actin filaments, the cells were stained with Alexa Fluor 488-conjugated Phalloidin (Cell Signaling, Technology, Danvers, MA, USA). The cells were then treated with 1 μg/mL Hoechst (Cell Signaling, Technology, Danvers, MA, USA) in order to label the nuclei. After each incubation, the samples were washed three times with PBS. In the end, the specimens were analyzed on glass slides using a DM 4000 B LED fluorescence microscope equipped with a DFC 450 C camera (Leica Microsystems, Wetzlar, Germany) with appropriate filters [120].

### *3.3.7 SaOs2 cell morphology*

The SaOs2 cell morphology was studied by SEM. For SEM studies, the cells were fixed after 1 and 3 days of interaction with samples. For fixation, 2.5% glutaraldehyde was used for 45 min at room temperature and washed two times with PBS. Samples were kept in PBS until the process of dehydration. This procedure involved successive immersion in 70%, 90%, and 100% ethanol (EtOH), 15 min twice for each concentration. Cells were then incubated by sequential incubation in 50%:50%, 25%:75%, and 0%:100% solutions of EtOH:hexamethyldisilazane (HMDS), two times for 3 min in each combination. The specimens were dried and metalized prior to the microscopy investigations. The metallization consisted of a 10 nm thin gold layer deposited by magnetron sputtering on the surface of specimens with a manual sputter coater (Agar Scientific, Essex, UK) [120].

### *3.3.8 X-ray Computed tomography*

While metallographic analysis reveals information about the microstructure and 2D pores or cracks, X-Ray Computer Tomography (XCT) discloses 3D defects in the bulk, with a resolution better than 1 micrometer and in a non-destructive manner.

The non-destructive analyses were conducted in the X-Ray Microtomography Laboratory of the National Institute for Lasers, Plasma and Radiation Physics (INFLPR), using a submicron X-Ray source with 225 kV maximum high voltage, 0.4 mm minimum object-focus distance and 170° X-Ray cone.

# 4. PARTS OF TITANIUM ALLOYS PRODUCED BY ADDITIVE MANUFACTURING

## 4.1 DEALING WITH DEFECTS IN TI GRADE 5 PARTS PRODUCED BY LMD

The aim of this study was to obtain final products fabricated by LMD without internal defects, such as pores, cracks, or non-melted inner regions. We will show that the scanning strategy for producing a part can be optimized in a matter of hours instead of days, as would be the case when using destructive analyses techniques.

The processing parameters, such as laser power, scanning speed and powder feed rate were previously optimized in order to obtain high density depositions free of defects such as pores, cracks or non-fusion powder particles [120]. They are provided in Table 4.1 and were preserved for all experiments. However, if depositions are conducted on larger areas or when using different scanning strategies, these conditions no longer ensure defects free depositions and a new study is necessary, this time taking into account hatch spacing and the distance between layers. The defects can be due to the higher temperature of the substrate caused by prolonged irradiation, which can cause higher rate evaporation, larger heat affected zones, deposition with non-uniform thickness, and change of metallographic structure or repeated dilatation-contraction cycles.

**Table 4.1. Optimized process parameters for tracing a clearly defined, parallel borders, single line of Ti6Al4V with the least residual material** [121]**.**

| Process parameter | Value |
|---|---|
| **Laser power** | 700 W |
| **Scanning speed** | 0.015 m/s |
| **Powder flow rate** | 3 gr/min |
| **Laser spot size** | 800 μm |
| **Layer thickness** | 2.5 mm |
| **Nozzle stand off** | 16 mm |
| **Ar shielding gas flow rate** | 10 l/min |
| **He shielding gas flow rate** | 3 l/min |

Bulk structures in shape of parallelepipeds with size of 30 mm × 15 mm × ΔZ mm (ΔZ varying function of the scanning strategy) were performed using eight different scanning patterns (Table 4.2).

**Table 4.2. Scanning strategy parameters** [121]**.**

| Sample | Offset between meander planes ΔZ [mm] | Hatch spacing [mm] | Overlap [%] |
|---|---|---|---|
| **S1** | 0.5 | 1 | 33 |

| | | | |
|---|---|---|---|
| **S2** | 0.5 | 1.25 | 20 |
| **S3** | 0.5 | 1.5 | 0 |
| **S4** | 0.75 | 0.5 | 66 |
| **S5** | 0.75 | 0.75 | 50 |
| **S6** | 1 | 1 | 33 |
| **S7** | 1 | 1.25 | 20 |
| **S8** | 1 | 1.5 | 0 |

Samples produced with the scanning strategies described in Table 4.2 were XCT scanned in order to identify defects that occurred during deposition. The samples were aligned with respect to the X-ray tomography system by placing the substrate interface parallel to the detector and the long side along direction of rotation. In other words, the Z axis from the sample coordinates is perpendicular to the X-ray detector.

The appearance of pore clusters is more probable among first several deposited layers that are nearest to the substrate (low $\Delta Z$ value). The thermo-dynamic stability is improving as the layer grows on the Z axis. Figure 4.1 shows the preferential pores positioning in a LMD deposited sample, scanned by XCT.

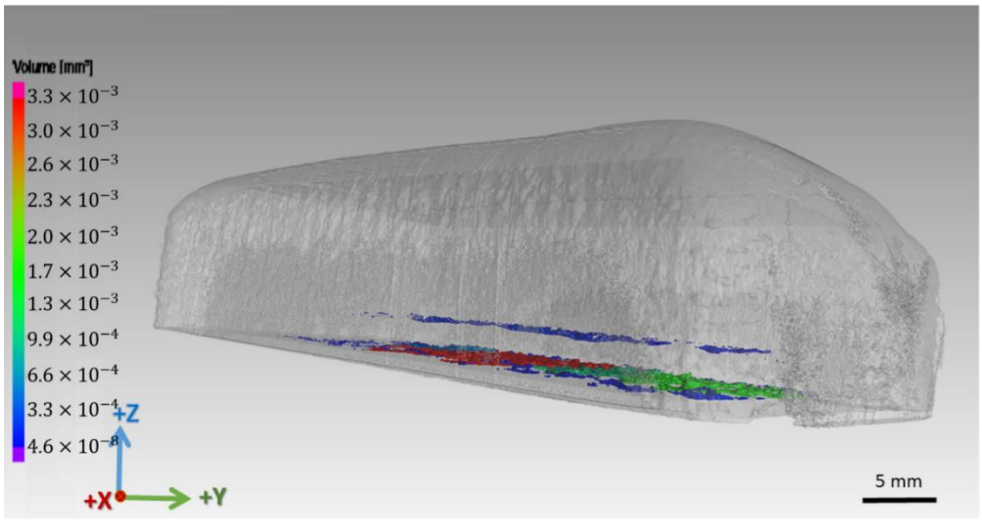


**Figure 4.1** 3D rendering on sample 4 highlighting the appearance of pore clusters, were the most predominant are near the substrate region [121].

Alternative solution to non-destructive monitoring and parameters tuning would be to accept samples with certain degree of porosity and to apply a post-processing heat treatment with hot isostatic pressing (HIP). Using HIP post-treatment, the porosity percentage decreased from 0.08% to 0.01% [122], [123]. However, with our solution, the percentage of porosity was an order of magnitude lower.

The parts quality monitoring technique by XCT is not limited to the LMD method or to the material used in this manuscript. It can be useful for assessing defects in metallic samples

with sizes of tens of centimeters obtained by casting, powder metallurgy or 3D printing by laser or electron beam [124]. The technique is also compatible with the most common metals used in metallurgy, so it can cover a wide range of applications.

### 4.2 Prototype orthopedic bone plates 3D printed by LMD

In this study, the LMD technique was chosen due to its good promise for the future development of large size implants, while minimizing the raw materials consumption. Furthermore, LMD is versatile, allowing its application for printing, coating, and alloying, and thus, opening the path towards innovation in the biomedical field. By LMD, Ti6Al4V composites can be synthesized in situ in combination with hard ceramic nanoparticles, such as TiC, in view of increasing its mechanical properties [125], [126]. There are numerous papers reporting LMD experiments starting from Ti6Al4V powders, especially for cladding or repairing of mechanical parts [127]–[129]. While SLM is the technique of choice for producing additive manufactured medical devices (such as hip or knee prostheses, dental implants, cranial meshes or plates for facial reconstruction [130]), the LMD literature is limited to physicochemical tests of LMD deposited biocompatible alloys [131]–[134].

The Ti6Al4V bone plates were produced from a micro-sized powder purchased from LPW Technology, Widnes, UK. The experimental set-up is described in detail in subsection 3.2.1. The particle size distribution analysis was performed on the basis of four SEM micrographs (Figure 4.2a-c). A representative EDXS spectrum is shown in Figure 4.2d, which highlights the high degree of the powder purity (at the sensitivity limit of the analysis technique), with only Ti, Al, and V peaks being evidenced.

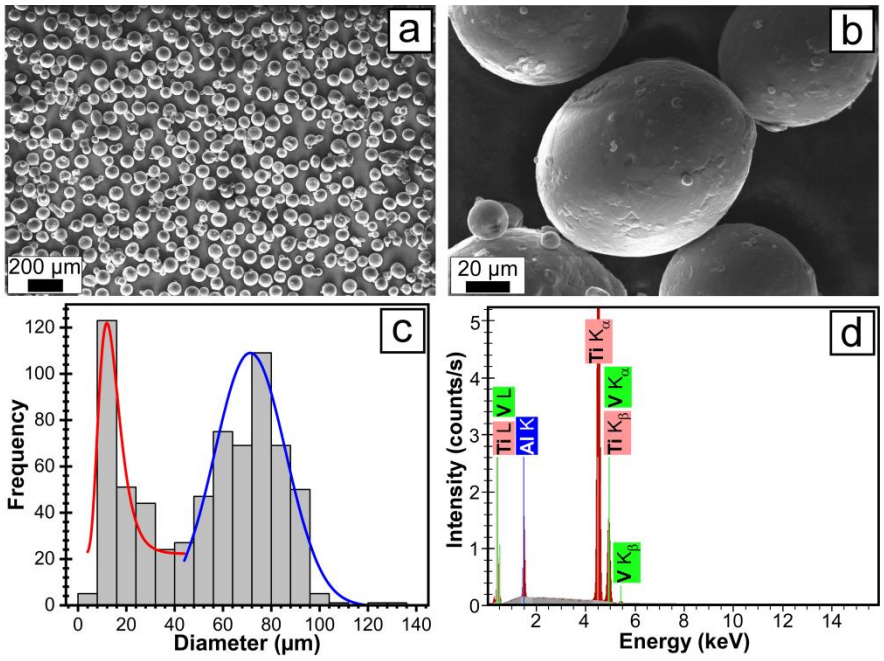


**Figure 4.2** (a) Overview of the SEM micrograph for Ti6Al4V powder used as source material for LMD manufacturing of prototype bone plates; (b) Detailed SEM morphology of the small micron-sized particles adhering to the 50–130 µm diameter large particles; (c) Particle size distribution histograms; (d) EDXS spectrum characteristic of the Ti6Al4V powder[120].

The final production step was of polishing by vibro-finishing. The surface polishing is produced by the relative movement between ceramic polishing chips and the bone plates, caused by the vibrations produced by the finishing machine. The final form of some bone plates is presented in Figure 4.3.

**Figure 4.3** Photo of bone plates in the final form produced by Laser Melting Deposition (LMD) and mechanically processed for dimensions and roughness requirements [120].

The cells proliferation results, as obtained by the MTS assay, are displayed in Figure 4.4a. Figure 4.4b presents the SEM morphology of SaOs2 cells grown onto the LMD printed Ti6Al4V. Further, the fluorescence microscopy images showed the degree of cellular surface coverage at 1 (Figure 4.4c) and 3 (Figure 4.4d) days after seeding. After three days, the SaOs2 cells proliferated and spread on the whole surface of the LMD printed Ti6Al4V biomaterial.

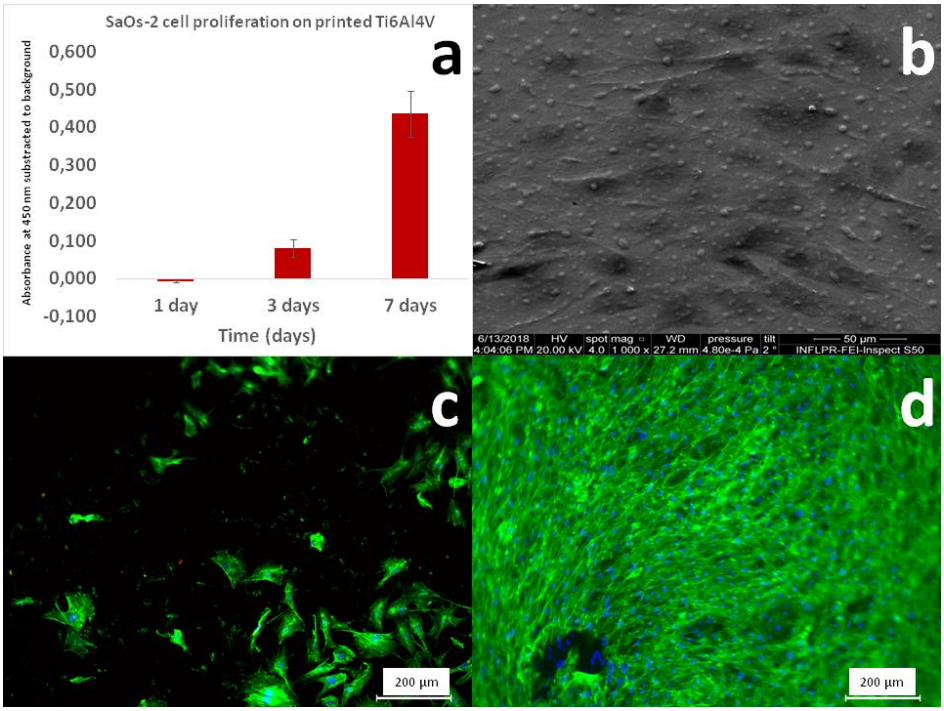


**Figure 4.4** (a) MTS results for the SaOs2 cells grown on Laser Melting Deposition (LMD) printed Ti6Al4V; (b) SEM micrograph of SaOs2 cells 3 days after seeding on LMD printed Ti6Al4V; Fluorescence microscopy images of SaOs2 cells cultivated for (c) 1 day and (d) 3 days on the surface of LMD printed Ti6Al4V [120].

## 4.3 3D-PRINTED IMPLANTS FUNCTIONALIZED WITH LITHIUM-DOPED BIOLOGICAL-DERIVED HYDROXYAPATITE COATINGS

The increase of life expectancy and the enhanced frequency of injuries and diseases are considered the most important causes for the escalating demand for dental and orthopedic devices. In this respect, the surface functionalization of implants with highly performant bioactive materials is currently of interest and necessary both for the prevention of failure and the prolongation of the bone implants' life. Usually, an implant can be manufactured from Ti or its medical-grade alloys. In this respect, additive manufacturing (AM) is a technology that allows for cost-effective and rapid production of complex three dimensional (3D) metallic parts and is gaining nowadays increased attention in the field of personalized medicine [135], [136].

### *Printing of Metallic Implants*

The laser melting deposition (LMD) technique was used for the manufacturing of three-dimensional (3D) metallic implants. A Ti6Al4V powder (with the particle size of <90 μm), further denoted as control, was used as precursor material. Implants were in "T"-shape (Figure 4.5a,b) and their dimensions are displayed in Figure 4.5a. It should be mentioned that, by using the LMD technique, the fabrication costs and manufacturing time of 3D metallic implants were significantly reduced.

### *Target Preparation*

The as-obtained Li-C and Li-P mixed powders were pressed at ~6 MPa in a 20 mm diameter mold. The resulting pellets were thermally treated in air, using an oven, for 4 h, at 700 °C. A heating rate of 20 °C/min and a cooling ramp of 5 °C/min were applied. Following this protocol, the fabrication of hard and compact targets was carried out.

### *Coating Fabrication*

PLD experiments were conducted inside a stainless-steel deposition chamber, in an ambient water vapor pressure of 50 Pa. The target-to-substrate separation distance was of 5 cm. Coatings were synthesized using a KrF* excimer laser source (COMPexPro 205, Coherent, Santa Clara, CA, USA, $\lambda$ = 248 nm, $\tau_{FWHM} \leq 25$ ns). The incident laser fluence was set at 3.5 J/cm$^2$ (with a corresponding pulse energy of 360 mJ). The laser beam was incident at 45° on the target surface. For the growth of one film, 15,000 consecutive laser pulses were applied. During the multi-pulse laser irradiation, the target was continuously rotated with 0.3 Hz and translated along two orthogonal axes, to avoid piercing and to obtain unidirectional plasma.

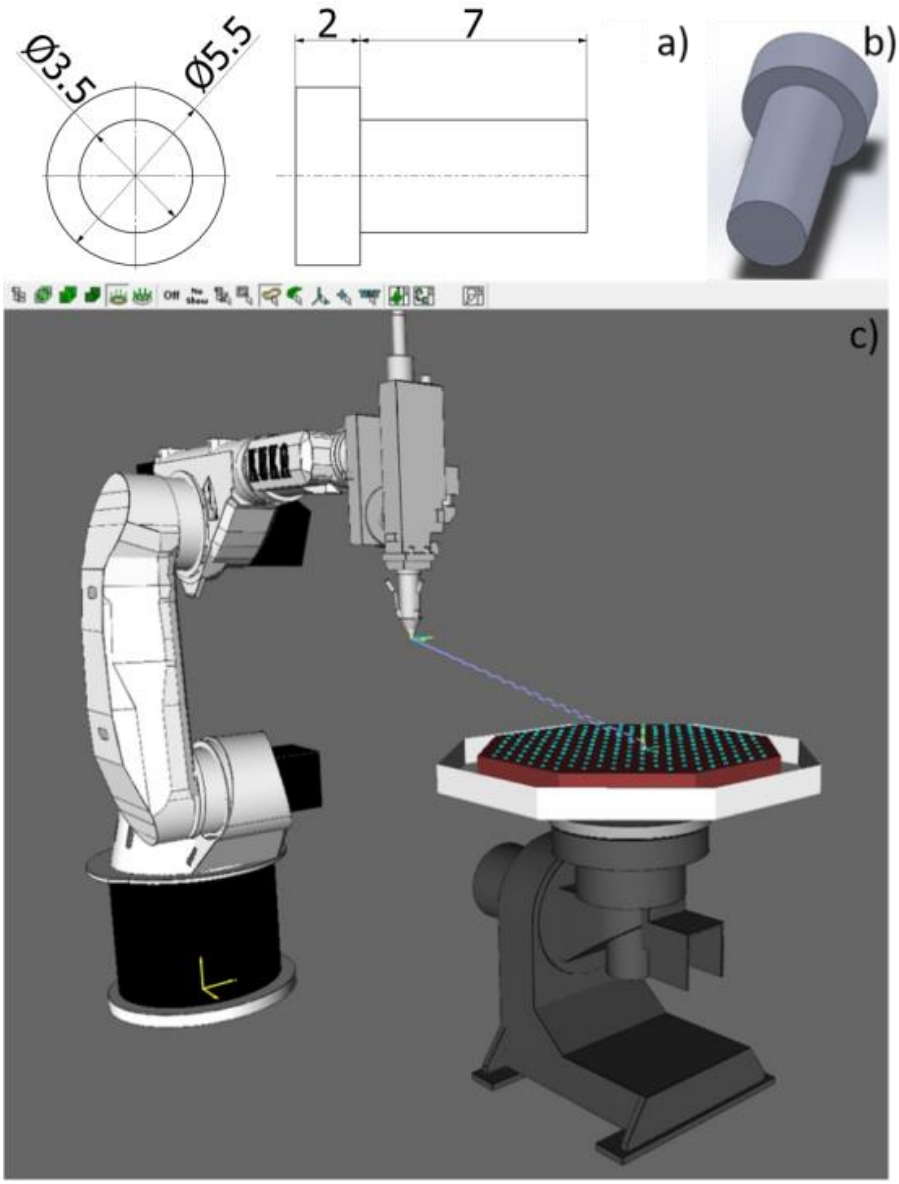


**Figure 4.5** (a) The technical drawing of the 3D metallic implant; (b) the 3D drawing of the implant; (c) the TruTops Cell® graphical software which generates the movement codes for the robotic arm [137].

### *Animals and Surgical Experimental Protocol*

For the in vivo experiments reported in this study, that took place in the biobase of the University of Medicine and Pharmacy (UMF), Craiova, Romania, a total of 26 skeletally-matured New Zealand White rabbits, aged six months and weighing between 3 and 3.5 kg were used.

Before surgery, the simple and functionalized 3D Ti implants were sterilized by autoclaving (at 120 °C, for 1 h).

The 26 rabbits were randomly assigned to two groups (n = 13 each). The 3D metallic implants were introduced into the femoral condyles [138] (two implants in each rabbit), using

the following sequence: at the level of the right femur, the 3D Ti implants functionalized with Li-C and/or Li-P coatings, and at the level of the left femur, the simple Ti implants (controls).

***Characterization of Simple and Functionalized Three-Dimensiomnal (3D) Ti Implants***

*Computed Tomography*

For this particular case the computer tomography investigations were performed using a Siemens CT scanner, operated at 130 kV, 90 mA, 0.5 mm section thickness and 0.3 mm section increment. The integration and total scan times were of 0.5 s and 2 min, respectively. For the evaluation of bone density, the Onis 2.3.5 software was used, and the inferred values were expressed on the Hounsfield tissue density scale (HU units). The area on the CT sections in which the tissue density was evaluated (also known as the region of interest), was always selected from the same region of the implant, for each performed measurement.

*Mechanical Testing*

Four weeks after the insertion of the 3D metallic implants, the rabbits were anesthetized (following the same protocol described above), and euthanized by intracardiac injection, using an overdose of sodium pentobarbital (100 mg/kg).

The measurement of the implants extraction force was performed by a tensile traction machine (model WDW, Time Group), which measures both the force and the elongation, and can operate with a maximum force of 5000 N. All tests were performed with a traction speed of 1 mm/min. The implant was positioned into the traction machine support by means of a hexagonal adapter attached with an adhesive on the exterior side of the Ti implant (Figure 4.6).

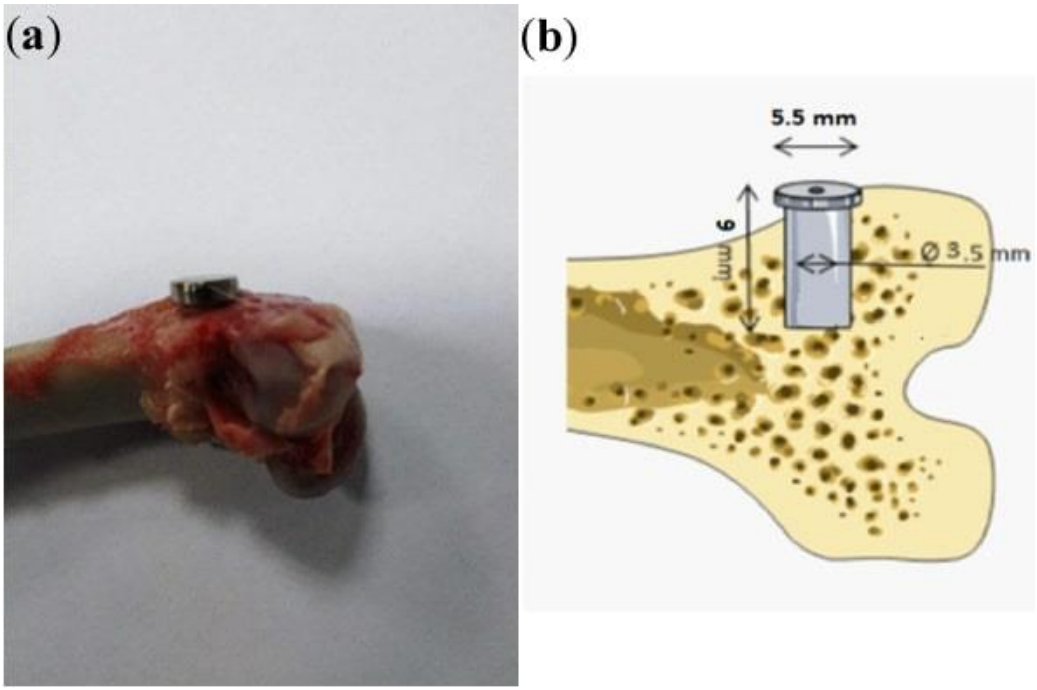


**Figure 4.6** (a) Photograph of the extracted bone; (b) schematic representation of the implant site [137].

After the extraction procedure, SEM examinations of simple and functionalized 3D Ti implants were carried out under two magnifications, i.e., 300× and 2000×, respectively (Figure 4.7).

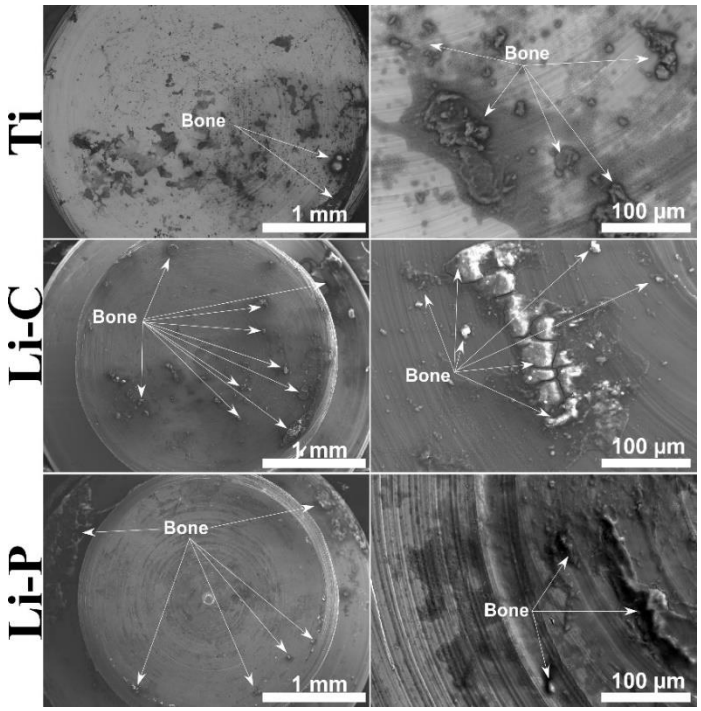


**Figure 4.7** SEM micrographs indicating bone detachment on the surface of a simple and functionalized (with Li-C and Li-P coatings) Ti implant, at 4 weeks after surgery [291].

All in all, the results of this preliminary in vivo assessment of the pulsed laser deposited BioHA doped with Li-C and Li-P coatings hold promise. Further and more insightful documentation on both the ingrowth characteristics' influence on the mechanical stability over various implantation time periods, and biomolecular analyses (i.e., related to gene expression of osteoblasts in contact with bone substitutes and/or HA [139]), will be considered. In addition, detailed in vivo studies, in which simple BHA coatings will be used as controls, will be imagined not only to assess the lithium effectiveness in in vivo experiments, but also to demonstrate their superiority also over the Ti commercial implants. All these investigations are necessary and should stand as the subject of a dedicated study which should start, however, from the results of this preliminary work

## 4.4 3D-PRINTED CRANIAL IMPLANTS SYNTHESIZED BY SLM AND COATED WITH ANIMAL ORIGIN HYDROXYAPATITE THIN FILMS

In a collaboration with hospital Dr. Oblu in Iasi, in Romania, we conducted a study dedicated to increasing of bioactivity of commercial Ti cranial implants by coating them with a thin layer of hydroxyapatite. Following this research, we took things further and produced cranial prostheses by 3D printing. The manufacturing consisted of two steps: first, the prosthesis was generated by 3D printing using the SLM method, while in a second step, a thin film was deposited by RF-MS from a target of biological apatite derived from bovine bones. The focus of this study was to assess for the first time the feasibility of depositing by RF-MS bioceramic

coatings of biogenic origin onto SLM custom-fabricated prosthesis. In this respect, morphological, compositional, structural and bio-functional interrogations were conducted for both the metallic part and the bioceramic coating.

Representative images of a Ti6Al4V cranial mesh before and after biofunctionalization with a Bio-HA thin film by RF-MS (Fig. 4.7).

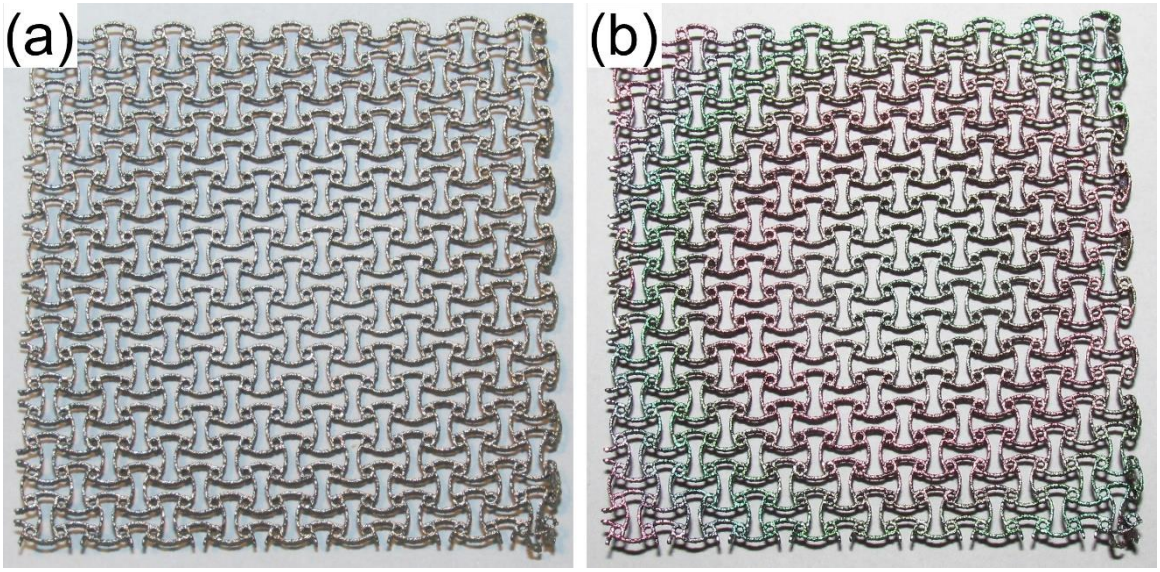


**Figure 4.7** (a) Uncoated and (b) Bio-HA sputtered cranial mesh of Ti6Al4V fabricated by SLM [140].

To determine the effect of Bio-HA coating on cell viability and proliferation, we have carried out an MTS test at 1, 3, and 7 days after cell seeding. As a control, a borosilicate glass coverslip was used, which is a cell culture standard [141]. The results are represented in Fig. 4.41 and they show an enhanced osteoblasts proliferation on the control up to 72h. However, after 168h, the Bio-HA sputtered substrate was found to encourage cells expansion, as indicated by a significant increase in MTS absorbance value. This result suggests a slower proliferation dynamic on Bio-HA at early time points which is compensated after cells reach semi-confluency.

The adhesion of SaOs-2 cells on the Bio-HA film and the control surface has been investigated by fluorescence microscopy (Fig. 4.8). The actin filaments were labelled in green to study the cytoskeleton organization, while the cell nuclei were represented in blue. As it can be seen from Fig. 4.4.2a,b, after one day of culture, cells have successfully attached on both substrates. However, in the case of the Bio-HA coating (Fig. 4.8a), cells have extended their membrane protrusions and changed their morphology to a more elongated phenotype. This difference in the cytoskeleton structure is more pronounced after three days of culture (Fig. 4.8c,d). Cells grown on the control material (Fig. 4.8d) elicit a more spread cell body compared to those on the Bio-HA substrate where they become rather elongated with multiple developed filipodia (Fig. 4.8c). However, taking into consideration the increased cell number detected after 7 days by MTS on the Bio-HA sputtered surface, we can conclude that this biomaterial is compatible with bone cell adhesion and expansion, which are key early steps important for osseointegration.

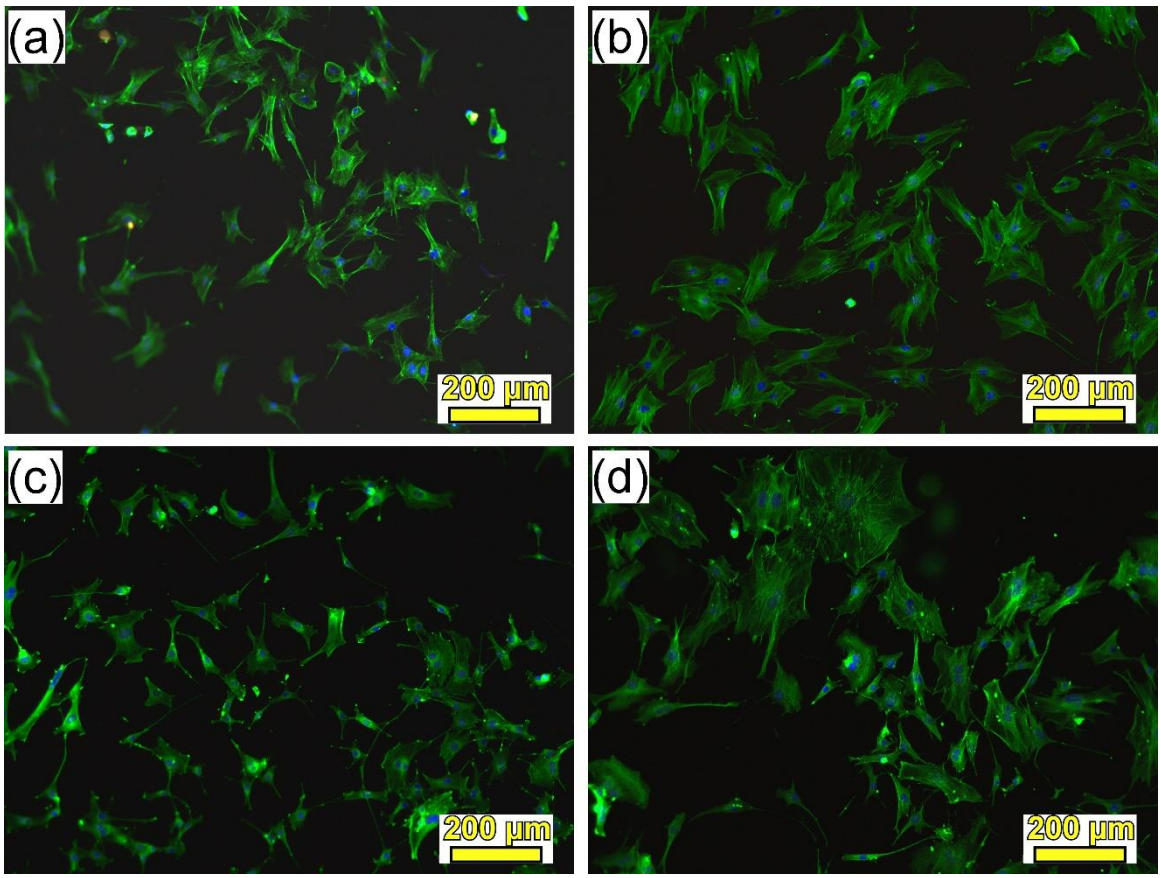


**Figure 4.8** Immunofluorescence microscopy images of SaOs-2 cells grown on the surface of the Bio-HA coated 3D printed Ti6Al4V substrates (a,c) and control substrate (b,d), after 1 (a,b) and 3 days (c,d) of seeding. The actin filaments are stained in green and the cell nuclei are labeled in blue. Scale bar = 200 µm [140].

Overall the physico-chemical properties and preliminary biological behavior of the sputtered Bio-HA films hold promise, and thus encourage us to further and more insightfully asses their potential from mechanical and biofunctional points of view.

# 5. CONCLUSIONS

## 5.1 GENERAL CONCLUSIONS

This thesis presents the most representative achievements in the matter of additive manufacturing of biocompatible metallic materials for personalized medical implants and devices of our group.

1. Our team first developed a mathematical model for three-jet powder flow and temperature distribution on the substrate's surface in the case of the LMD process. Initially, the Gaussian powder stream was simulated. Following on, the powder flow was added coaxially with the moving laser beam to analyze the effect of powder addition on the temperature distribution of the substrate. Additionally, an analytical formula to estimate the laser beam energy attenuation has been obtained. The particles' inflight and within the melt-pool heating times were controlled to avoid excessive heating and possible transformation into vapors and plasma. This study provided a cost- and time-effective way in the LMD process by adjusting the operating parameters to gain an optimal solution for powder debits and resultant energy.
2. A quality improvement study for Laser Melting Deposition of Ti6Al4V parts was undertaken in order to completely eliminate internal defects. X-Ray Computed Tomography proved to be an invaluable tool for non-destructive characterization of the bulk for defects assessment. Two types of pores were identified by XCT in LMD produced samples: some spherical, caused by gases produced by local evaporation and some polyhedral ones caused by lack of superposition between the lines that produced the samples and a supplemental contour line traced or correction of the sample borders. The circular pores were concentrated close to the interface with the substrate. They were aligned along scanning direction forming parallel rows of voids. The larger the hatch spacing the lower the number of pores. By increasing the hatch spacing to 1.5 mm, the pores disappeared completely. For complete elimination of polyhedral pores from the borders of the samples, the contour line was partially superposed over the meander. XCT revealed that an overlap of 50% between the contour line and the meander was sufficient to eliminate the pores.
3. Orthopedic bone plates of Ti6Al4V with shape and dimensions similar to the commercial laser cut ones, starting from powder materials, were printed by LMD. By optimizing the laser and scanning parameters, dense depositions with no porosity or cracks and with excellent compositional uniformity were obtained. The design of the trajectory followed by the laser beam proved essential in obtaining shapes that respect the dimensions and aspect of the technical drawings. The incipient 3D shapes obtained by 3D printing were further engineered by cutting, drilling and polishing in order to obtain the final bone plates. The metallographic analyses showed that the samples lack porosity or defects usually caused by rapid heating/cooling cycles. The metallographic attack revealed $\alpha+\beta$ grains with a cubic phase matrix in which hexagonal $\alpha$ grains proliferated. The micro-hardness of the LMD printed Ti6Al4V was higher than that of

the casted material, probably due to a basket-like interweaved grain structure, finer than the standard Widmanstatten structure of a casted material. The LMD printed Ti6Al4V alloy was biocompatible. There were no surface features or compositional deviations that could cause a negative response from cells. The in vitro assays showed that the osteoblast-like cells survived and proliferated well in the following seven days after seeding.

4. Pulsed laser deposition was used for the synthesis of biological-derived hydroxyapatite doped with lithium carbonate (Li-C) and phosphate (Li-P) coatings. The Li-C and Li-P structures were investigated in vivo, as coatings on 3D metallic implants which were inserted in rabbits' femoral condyles, for 4 and 9 weeks, respectively. The bone density measurements of the functionalized implants, performed either at 4 or 9 weeks, showed superior values in comparison to simple (control) ones. The inferred detachment force values of the functionalized implants were ~2 times higher than those registered for the corresponding control ones. When referring to longer implantation time periods (i.e., 9 weeks), the extraction test results indicated improved bonding strength values (~5 times higher) of the functionalized implants as compared to the same structures, but corresponding to an implantation time period of 4 weeks. Therefore, the mechanical testing is indicated as a promising tool to investigate the early phase of 3D Ti implants attachment to bone.
5. 3D cranial meshes of Ti6Al4V were successfully manufactured by SLM. The microstructure of Ti6Al4V deposited by SLM was martensitic α'. The irradiation parameters were optimized in order to obtain shapes without defects, such as pores or cracks and with homogeneous distribution of alloy elements in their volume. In a second technological step, the implants produced by SLM were coated by radio-frequency magnetron sputtering with a ~600 nm layer of hydroxyapatite derived from biogenic sustainable resources (i.e. calcined cortical bovine bones), which could constitute a cost-efficient, environmental-friendly and highly promising biofunctional solution. The Bio-HA sputtered films elicited promising biological performances:
    - ✓ Chemical stability in simulated physiological solutions (after 21 days the film thickness was reduced by ~14% in SBF and ~5% in FBS-supplemented McCoy's 5A medium);
    - ✓ Biomineralization capacity (Bio-HA generated the formation of spherulitic deposits of biomimetic calcium phosphates in contact with both types of simulated physiological solutions);
    - ✓ Absent cytotoxicity;
    - ✓ Optimal osteoblast cell proliferation and adhesion.

## 5.2 PERSONAL CONTRIBUTIONS

The objective of this thesis was to fabricate medical implants using additive manufacturing techniques. In this sense an analytical model was developed for a better understanding of the parameters influence during the process, an optimization study was conducted in order to obtain defect free samples and three different medical devices were fabricated.

- ✓ The analytical models obtained based on mathematical equations used in practice were compared with experimental results provided by myself. I recorded the powder flow of a three-beam nozzle via a high-speed imaging camera (AX100, Photron, Tokyo, Japan). The shape and the width of the powder stream were highlighted using "Image J" software (1.53a, National Institute of Health and the Laboratory for Optical and Computational Instrumentation, Wisconsin, USA. The process parameters used in the analysis were established based on experimental data delivered by me. I contributed on writing – review the manuscript [112].
- ✓ The paper about optimization of the scanning strategy in order to obtain defect free samples that were analyzed via XCT was concept by me. I was responsible with the LMD experiments which includes process parameters optimization, generate the program of the robot movement, fabrication and preparing the samples for XCT analysis. I interpreted the results, wrote the original draft and prepared the review [121].
- ✓ I was responsible of 3D medical devices fabrication starting with the conceptualization of the CAD model. I optimized the process parameters and scanning strategies in order to get parts that respect the technical drawings. I generated the CNC programs for the robot movement, I prepared the samples for the metallographic analysis and I evaluated the microstructure using an optical microscope. I was in charge of post-processing steps needed to obtain the desired surface finishing in case of orthopedic bone plates [120] and medical implants fasteners [137].

Personal contributions can be summarized as follows:

- → Development of mathematical models – experimental input data, recording powder flow shape via high speed camera and analysis of powder flow distribution.
- → 3D printed samples – design, programming the robot movement for sample manufacturing, process parameters optimization, porosity evaluation and methodology.
- → Orthopedic bone plates – design of CAD model, programming the robot movement, process parameters optimization, part fabrication, metallographic analyses, characterization of powder and bulk material, methodology.
- → Cranial meshes – design of CAD model, metallographic analyses, characterization of powder and bulk material, methodology.
- → Medical implants fasteners - design of CAD model, programming the robot movement, process parameters optimization, part fabrication, post-processing.

The results of the thesis have been exposed in 12 scientific ISI articles (Appendix A), 3 submitted patent demands, 1 technical documentation (Appendix B), 12 oral presentations at national/international conferences (Appendix C) and 5 poster presentations at national/ international conferences (Appendix D). The total **IF** and **AIS** score amounts to **29.52**, respectively **5.14**.

## 5.3 FUTURE WORK

In the near future, there are several directions in 3D printing that will be tackled by our team, in which the shape will be quite prominent:

- One of our main topics of research will be the testing of ceramic substrates on which metallic parts can be built by LMD. All groups are dealing with 3D printing of metallic parts use metallic substrates. This means that at the end of the printing process, the part has to be detached from the substrate by cutting. In case of Ti and it's alloys, the hardness is 40% higher than in case of stainless steel and cutting it is time consuming. Moreover, the cutting tools can be broken during the cutting process, thus increasing the fabrication costs. After cutting, the part has to be post-processed to smoothen the in-aesthetic bottom side. Our aim is to find a refractory ceramic material compatible with the metallic structure deposited by 3D printing (in order to avoid defects at the interface), that can be easily broken, in order to release the printed part. Studies are underway in the framework of the Nucleus Project of INFLPR.
- Another subject of interest for me is the 3D printing of Metal Matrix Composites (MMC). These are materials with a metallic matrix and a dispersed phase of particles. By using light matrices and hard particles for reinforcements, one can obtain materials with amazing mechanical properties and in the same time with a very light mass. I envisage two distinct paths towards reaching this objective: I) the starting material will be a mixed powder of matrix and dispersed phase materials that will be blown into the laser spot from a single powder feeder and II) matrix powder will be inserted into a powder feeder, while dispersed phase powder will be inserted into a second powder feeder and they will be blown into the laser spot concomitantly with different debit rates in order to reach a desired proportion of dispersed phase into the matrix.
- In a new project of our group, the main research line will be to produce parts by 3D printing, with enhanced surface topology, in order to minimize their mass and to increase their resistance to mechanical solicitations. The user indicates in the CAD software the constrictions for the part and the areas that will have to withstand mechanical solicitations. Based on this information, the software will calculate the optimal shape that will require the least amount of material, but will provide the highest resistance to the required applied forces. The resulting shapes can be often convoluted, making their production by conventional casting techniques quite challenging. We will try to produce such shapes by 3D printing, using the LMD method.

Finally, my main goal is to become independent in my research. My focus will be to apply and win projects in the national competitions, which will allow me to become familiarized with the management of research. They will also provide freedom of research on my own thematic and the possibility to become an accomplished researcher, by slowly gathering and guiding a small research team.

# APPENDIX

## A. LIST OF PUBLICATIONS

This list contains Article Influence Score (AIS) from www.eigenfactor.org and the Impact Factor (IF) from Web of Science (v. 5.32) Web of Science Core Collection, if applicable.

1. Mahmood MA; Popescu AC; Oane M; **Chioibasu D**; Popescu-Pelin G; Ristoscu C; Mihailescu IN, Grain refinement and mechanical properties for AISI304 stainless steel single-tracks by laser melting deposition: Mathematical modelling versus experimental results, Results in Physics, vol. 22, pp. 103880, 2021, **IF=4.019, AIS = 0.491**
2. Mahmood MA; Popescu AC; Oane M; Ristoscu C; **Chioibasu D**; Mihai S, Mihailescu IN, Three-Jet Powder Flow and Laser–Powder Interaction in Laser Melting Deposition: Modelling Versus Experimental Correlations, Metals vol. 10, pp. 1113, 2020, **IF=2.1170, AIS = 0.343**
3. **Chioibasu D;** Mihai S; Mahmood MA; Lungu M; Porosnicu I; Sima A; Dobrea C; Tiseanu I; Popescu AC, Use of X-ray Computed Tomography for Assessing Defects in Ti Grade 5 Parts Produced by Laser Melting Deposition. Metals, vol. 10, pp. 1408, 2020, **IF=2.1170, AIS = 0.343**
4. Duta, L.; Neamtu, J.; Melinte, R.P.; Zureigat, O.A.; Popescu-Pelin, G.; **Chioibasu, D.;** Oktar, F.N.; Popescu, A.C. In Vivo Assessment of Bone Enhancement in the Case of 3D-Printed Implants Functionalized with Lithium-Doped Biological-Derived Hydroxyapatite Coatings: A Preliminary Study on Rabbits. Coatings, vol. 10, pp. 992, 2020, **IF=2.4360, AIS = 0.376**
5. **Chioibasu D**; Călin B; Popescu A; Puşcaş N; Klobčar, INVESTIGATION OF DISSIMILAR LASER WELDING OF STAINLESS STEEL 316L TO ALUMINIUM A1050 IN LAP JOINTS CONFIGURATION, , U.P.B. Sci. Bull., Series A vol. 82 iss.1, pp, 271–278, 2020, **IF = 0.4610, AIS = 0.094**
6. **Chioibasu D**; Călin B; Popescu A; Puşcaş N; Klobčar D, Optimization of laser butt-welding of stainless steel 316L using response surface methodology, U.P.B. Sci. Bull., Series A, Vol. 82, Iss. 2, 2020, **IF = 0.4610, AIS = 0.094**
7. **Diana Chioibasu**, Alexandru Achim, Camelia Popescu, George E. Stan, Iuliana Pasuk, Monica Enculescu, Stefana Iosub, Liviu Duta, Andrei Popescu, Prototype Orthopedic Bone Plates 3D Printed by Laser Melting Deposition, Materials vol. 12, iss. 6, pp. 906 2019, **IF = 2.9720, AIS = 0.607**
8. **Chioibasu D**; Duta L; Popescu-Pelin G; Popa N; Milodin N; Orobeti (Iosub) S; Marinela Balescu L; Galca AC; Popa AC; Oktar FN; Stan GE and Popescu AC, Animal Origin Bioactive Hydroxyapatite Thin Films Synthesized by RF-Magnetron Sputtering on 3D Printed Cranial Implants, Metals vol. 9, iss. 12, pp 1332, 2019, **IF = 2.2590, AIS = 0.361**
9. Paun IA; Popescu RC; Mustaciosu CC; Zamfirescu M; Calin BS; Mihailescu M; Dinescu, M; Popescu A; **Chioibasu D**; Sopronyi M; Luculescu CR; Laser-direct writing by two-photon polymerization of 3D honeycomb-like structures for bone regeneration, BIOFABRICATION vol.10, iss. 2, pp. 25009, 2018, **IF = 6.8380, AIS =1.2**
10. **Chioibasu D**; Sima A; Dobrea C; Paun I; Popescu A; Luculescu C; Tiseanu I; Puscas N; "NON-DESTRUCTIVE OPTICAL ANALYSIS OF POROSITY CONTENT DURING Yt: YAG LASER WELDING OF Al Alloy 1050 USING X-RAY MICRO-

TOMOGRAPHY", U.P.B. Sci. Bull., Series A, Vol. 79, Iss. 4, 2017, **IF = 0.2790, AIS =0.094**

11. Luculescu CR; Acasandrei AM; Mustaciosu CC; Zamfirescu M; Dinescu M; Calin BS; Popescu A; **Chioibasu D**; Cristian D; Paun IA; "Electrically responsive microstructured polypyrrole-polyurethane composites for stimulated osteogenesis" Applied Surface Science, Vol. 433, iss 1, Pag 166-176, 2017, **IF = 3.3870, AIS = 0.627**
12. Popescu C; Cristea D; Bita B; Cristescu R; Craciun D; **Chioibasu D**; Luculescu C; Paun I; Duta L and Popescu AC, "An Experimental Study on Nano-Carbon Films as an Anti-Wear Protection for Drilling Tools", Coatings, vol. 7, iss. 12, pp. 228, 2017, **IF = 2.1750, AIS = 0.51**

**Total: IF = 29.52, AIS = 5.14**

B. LIST OF PATENTS AND TECHNICAL DOCUMENTATIONS

1. **Diana CHIOIBASU**, Sabin MIHAI, Liviu DUTA, Andrei C. POPESCU, "Tehnologie de fabricație aditivă a unor dispozitive de fixare pentru implanturi metalice prin metoda „Depunere Laser prin Topire" A/00214/22.04.2020;
2. **Diana CHIOIBASU**, Sabin MIHAI, Raluca IVAN, Andrei C. POPESCU, "Disc de frână acoperit cu un strat metalic pentru protecție la coroziune și uzură și metodă de obținere a acestuia", A/00550/ 02.09.2020;
3. **Diana CHIOIBASU**, Andrei POPESCU "Metoda pentru cresterea rezolutiei de scriere si imprimare 3D in cazul depunerii laser prin topire"A/00341/22.05.2018;
4. **Diana CHIOIBASU**, Sabin MIHAI, Andrei C. POPESCU – "Tehnologie de acoperire a discurilor de frana prin placare laser" – Transfer de cunostinte catre compania S.C. Optoelectronica-2001 S.A.

## C. LIST OF ORAL PRESENTATIONS

1. S. Mihai, **D. Chioibasu**, A. C. Popescu, “Metallic Implants 3D Printed by Additive Manufacturing” EmergeMAT 3RD International Conference on Emerging Technologies in Materials Engineering , 29-30 October 2020, Bucharest;
2. **D. Chioibasu**, Design, manufacturing and testing of Ti6Al4V prostheses printed by laser melting deposition, EuroNanoForum 2019, 12-14 June 2019, Bucharest, Romania;
3. **D. Chioibasu**, Prototype orthopaedic prostheses 3D printed by laser melting deposition (LMD), EmergeMAT 2ND International Conference on Emerging Technologies in Materials Engineering, 6-8 November 2019, Bucharest, Romania;
4. **D. Chioibasu**, Andrei Popescu, Marc Leparoux, Removal of excessive spatter generated during laser welding of metal matrix nanocomposites,International Conference on Renewable Energy and Energy Conversion ICREEC’2019 USTO-MB 11 - 13 November 2019, Oran, Algeria;
5. **D. Chioibasu**, A.C. Popescu, Prototype cranial mesh prostheses produced by laser additive manufacturing, European Materials Research Society (E-MRS) , 27-31 May 2019, Nice, France;
6. **D. Chioibasu**, A.C. Popescu, Computer-aided design choices for increasing resolution during metallic prostheses 3D printing,The 7th Global Conference on Materials Science and Engineering (CMSE2018), oct 30 - 6 nov, 2018, Xi'an, China;
7. **D. Chioibasu**, A.C. Popescu, Study on the characterization of 3D walls of Ti6Al4V structures made by Laser Melting Deposition (LMD),7th International Summer School on Trends and new developments in Laser Technology 27 – 31 August 2018, Dresden, Germany;
8. A.C. Popescu, **D. Chioibasu**, Design, manufacturing and testing of Ti6Al4V cranial mesh prostheses printed by laser melting deposition,The 7th Global Conference on Materials Science and Engineering (CMSE2018), oct 30 - 6 nov, 2018, Xi'an, China;
9. **D. Chioibasu**, M. Zamfirescu, V. Ciobanu , A. Sima, C. Dobrea , I. Tiseanu, "Pulsed Laser Welding of Dissimilar Materials (Al-CuNi) in Overlapping Joint Configuration for Electric Vehicles Batteries"2nd International Conference on: Applied Physics, System Science and Computers, 27-29 September, 2017 Dubrovnik, Croatia;
10. **D. Chioibașu**, D. Klobčar, D. Sporea, S. Smolej and A. Nagode, "Investigation of dissimilar laser welding of stainless steel to aluminium in lap joints configuration" Conferinta Anuala a Facultatii de fizica, Universitatea Bucuresti, 2017, Bucharest, Romania;
11. **D. Chioibașu**, D. Klobčar, D. Sporea, M. Jezeršek, J. Tušek, M. Kos, "Application of response surface methodology for optimization of fibre laser welding of stainless steel 316 L"Conferinta Anuala a Facultatii de fizica, Universitatea Bucuresti, 2017, Bucharest, Romania;
12. **D. Chioibasu**, N.Puscas, "Investigation of laser welding of aluminium A1050 in a butt joint configuration" Sesiunea de Comunicari Stiintifice Studentesti a Studentilor Doctoranzi , UPB 2017, Bucharest, Romania.

## D. LIST OF POSTER PRESENTATIONS

1. **D. Chioibasu** , S. Mihai , M. A. Mahmood , I. Tiseanu, M. Lungu, I. Porosnicu, A. C. Popescu, Porosity Characterization of Samples 3D Printed by Laser Melting Deposition Using X-Ray Computer Tomography, Emergemat 3rd International Conference On Emerging Technologies In Materials Engineering , 29-30 October 2020, Bucharest, Romania;
2. M. A. Mahmood, A.C. Popescu, M. Oane, C. Ristoscu, **D. Chioibasu**, S. Mihai , I. N. Mihailescu , 3-Jet Powder Flow and Laser-Powder Interaction in Laser Melting Deposition: Modelling Versus Experimental Correlations, Emergemat 3rd International Conference On Emerging Technologies In Materials Engineering, 29-30 October 2020, Bucharest, Romania;
3. S. Mihai, **Diana Chioibasu**, A. Popescu, M. Leparoux, Behavior of an aluminum based metal matrix nanocomposite during irradiation with high power laser pulses, EmergeMAT-2ND International Conference on Emerging Technologies in Materials Engineering, 6-8 November 2019, Bucharest, Romania;
4. **D. Chioibasu**, S. Iosub, F. Sima, A.C. Popescu, Design and fabrication of Ti6Al4V tibia prostheses using 3D printing by Laser Melting Deposition, Laser Ignition Summer School 2018, 02-06 July 2018, Sibiu, Romania
5. **D. Chioibasu**, M. Zamfirescu, V. Ciobanu , A. Sima, C. Dobrea , I. Tiseanu, "Pulsed Laser Welding of Dissimilar Materials (Al-CuNi) in Overlapping Joint Configuration for Electric Vehicles Batteries"Laser Ignition Summer School 2017, 19-22 July 2017, Brasov, Romania.

## REFERENCES


[1] P. Peyre, M. Dal, S. Pouzet, and O. Castelnau, "Simplified numerical model for the laser metal deposition additive manufacturing process," *J. Laser Appl.*, vol. 29, no. 2, p. 022304, May 2017.

[2] T. H. Maiman, "Stimulated optical radiation in ruby," *Nature*, vol. 187, pp. 493 –494, 1960.

[3] G. D. Chioibasu and C. Viespe, "Laser cutting of small-diameter holes in aluminum and carbon-steel sheets," *Rom. Reports Phys.*, vol. 67, no. 4, pp. 1616–1624, 2015.

[4] A. H. Elsheikh, W. Deng, and E. A. Showaib, "Improving laser cutting quality of polymethylmethacrylate sheet: Experimental investigation and optimization," *J. Mater. Res. Technol.*, vol. 9, no. 2, pp. 1325–1339, Mar. 2020.

[5] I. Sakaev and A. A. Ishaaya, "Diode laser assisted oxygen cutting of thick mild steel with off-axis beam delivery," *Opt. Laser Technol.*, vol. 138, p. 106876, Jun. 2021.

[6] H. Wang *et al.*, "Magnet-assisted laser hole-cutting in magnesium alloys with and without water immersion," *J. Manuf. Process.*, vol. 61, pp. 539–560, Jan. 2021.

[7] M. Li, L. Chen, and X. Yang, "A feasibility study on high-power fiber laser cutting of thick CFRP laminates using single-pass strategy," *Opt. Laser Technol.*, vol. 138, p. 106889, Jun. 2021.

[8] A. Kanyilmaz, "The problematic nature of steel hollow section joint fabrication, and a remedy using laser cutting technology: A review of research, applications, opportunities," *Engineering Structures*, vol. 183. Elsevier Ltd, pp. 1027–1048, 15-Mar-2019.

[9] N. Levichev, G. Costa Rodrigues, V. Vorkov, and J. R. Duflou, "Coaxial camera-based monitoring of fiber laser cutting of thick plates," *Opt. Laser Technol.*, vol. 136, p. 106743, Apr. 2021.

[10] M. Boujelbene *et al.*, "Effect of cutting conditions on surface roughness of machined parts in CO2 laser cutting of pure titanium," *Mater. Today Proc.*, Jan. 2021.

[11] M. M. Quazi *et al.*, "Current research and development status of dissimilar materials laser welding of titanium and its alloys," *Optics and Laser Technology*, vol. 126. Elsevier Ltd, p. 106090, 01-Jun-2020.

[12] B. Acherjee, "Hybrid laser arc welding: State-of-art review," *Optics and Laser Technology*, vol. 99. Elsevier Ltd, pp. 60–71, 01-Feb-2018.

[13] M. Mehrpouya, A. Gisario, and M. Elahinia, "Laser welding of NiTi shape memory alloy: A review," *Journal of Manufacturing Processes*, vol. 31. Elsevier Ltd, pp. 162–186, 01-Jan-2018.

[14] M. Hietala, M. Ali, A. Khosravifard, M. Keskitalo, A. Järvenpää, and A. Hamada, "Optimization of the tensile-shear strength of laser-welded lap joints of ultra-high strength abrasion resistance steel," *J. Mater. Res. Technol.*, Feb. 2021.

[15] M. Saravana Kumar and S. Rashia Begum, "Simulation of hybrid (LASER-TIG) welding of stainless steel plates using design of experiments," *Mater. Today Proc.*, Nov. 2020.

[16] W. Suder, S. Ganguly, S. Williams, and B. Y. B. Yudodibroto, "Penetration and mixing of filler wire in hybrid laser welding," *J. Mater. Process. Technol.*, vol. 291, p. 117040, May 2021.

[17] C. Wang, W. Suder, J. Ding, and S. Williams, "Wire based plasma arc and laser hybrid additive manufacture of Ti-6Al-4V," *J. Mater. Process. Technol.*, p. 117080, Feb. 2021.

[18] A. Aminzadeh, S. S. Karganroudi, and N. Barka, "A novel approach of residual stress prediction in ST-14/ST-44 laser welded blanks; mechanical characterization and experimental validation," *Mater. Lett.*, vol. 285, p. 129193, Feb. 2021.

[19] C. Li and K. Wang, "Effect of welding temperature and protein denaturation on strength of laser biological tissues welding," *Opt. Laser Technol.*, vol. 138, p. 106862, Jun. 2021.

[20] K. S. Mao *et al.*, "Effect of laser welding on deformation mechanisms in irradiated austenitic stainless steel," *J. Nucl. Mater.*, vol. 528, p. 151878, Jan. 2020.

[21] E. Di Francia *et al.*, "Novel procedure for studying laser-surface material interactions during scanning laser ablation cleaning processes on Cu-based alloys," *Appl. Surf. Sci.*, vol. 544, p. 148820, Apr. 2021.

[22] X. Li *et al.*, "Improvement of corrosion resistance of H59 brass through fabricating superhydrophobic surface using laser ablation and heating treatment," *Corros. Sci.*, vol. 180, p. 109186, Mar. 2021.

[23] G. Hull, E. D. McNaghten, P. Coffey, and P. Martin, "Isotopic analysis and plasma diagnostics for lithium detection using combined laser ablation–tuneable diode laser absorption spectroscopy and laser-induced breakdown spectroscopy," *Spectrochim. Acta - Part B At. Spectrosc.*, vol. 177, p. 106051, Mar. 2021.

[24] Y. Rong, Y. Huang, M. Li, G. Zhang, and C. Wu, "High-quality cutting polarizing film (POL) by 355 nm nanosecond laser ablation," *Opt. Laser Technol.*, vol. 135, p. 106690, Mar. 2021.

[25] B. Liu, G. Mi, and C. Wang, "Study on surface state and thermophysical properties of TA15 alloy by laser ablation," *J. Manuf. Process.*, vol. 62, pp. 483–490, Feb. 2021.

[26] S. Loganathan, S. Santhanakrishnan, R. Bathe, and M. Arunachalam, "FTIR and Raman as a noninvasive probe for predicting the femtosecond laser ablation profile on heterogeneous human teeth," *J. Mech. Behav. Biomed. Mater.*, vol. 115, p. 104256, Mar. 2021.

[27] G. Lu, U. Trdan, Y. Zhang, and J. L. Dulaney, "The distribution regularity of residual stress on a metal surface after laser shock marking," *Mech. Mater.*, vol. 143, p. 103310, Apr. 2020.

[28] C. Leone, E. Bassoli, S. Genna, and A. Gatto, "Experimental investigation and optimisation of laser direct part marking of Inconel 718," *Opt. Lasers Eng.*, vol. 111, pp. 154–166, Dec. 2018.

[29] M. G. Naumova, I. G. Morozova, and P. V. Borisov, "Investigating the features of color laser marking process of galvanic chrome plating in order to create a controlled color image formation at given marking," in *Materials Today: Proceedings*, 2019, vol. 19, pp. 2405–2408.

[30] I. Shivakoti, G. Kibria, and B. B. Pradhan, "Predictive model and parametric analysis of laser marking process on gallium nitride material using diode pumped Nd:YAG laser," *Opt. Laser Technol.*, vol. 115, pp. 58–70, Jul. 2019.

[31] X. Sun, W. Wang, X. Mei, A. Pan, J. Zhang, and G. Li, "Femtosecond laser dot-matrix marking on nickel-based alloy using a simple diaphragm-based spatial shaped modulation: Size and position control of marking units with high recognition rate," *J. Alloys Compd.*, vol. 835, p. 155288, Sep. 2020.

[32] Y. Lu *et al.*, "A review on diamond-like carbon films grown by pulsed laser deposition," *Applied Surface Science*, vol. 541. Elsevier B.V., p. 148573, 01-Mar-2021.

[33] T. Guo *et al.*, "Preparation and characterization of CuSbSe2 thin films deposited by pulsed laser deposition," *Mater. Sci. Semicond. Process.*, vol. 127, p. 105716, Jun. 2021.

[34] D. Wang *et al.*, "Effect of pulse bias voltages on performance of CdTe thin film solar cells prepared by pulsed laser deposition," *Sol. Energy*, vol. 213, pp. 118–125, Jan. 2021.

[35] I. Saadon Najm, S. Mahmood Kadhim, and A. Abdulkhaleq Alwahib, "Investigation the CuS thin film prepared by pulsed laser deposition," *Mater. Today Proc.*, Feb. 2021.

[36] Y. Lu *et al.*, "Arrays of needle-like TiO2/CdS nanorod heterostructure photoelectrodes with enhanced photoelectrochemical properties fabricate by pulsed laser deposition," *Vacuum*, vol. 184, p. 109985, Feb. 2021.

[37] X. Shi *et al.*, "Thermal behavior and fluid dynamics within molten pool during laser inside additive manufacturing of 316L stainless steel coating on inner surface of steel tube," *Opt. Laser Technol.*, vol. 138, p. 106917, Jun. 2021.

[38] Q. Yu, C. Wang, Z. Zhao, C. Dong, and Y. Zhang, "New Ni-based superalloys designed for laser additive manufacturing," *J. Alloys Compd.*, p. 157979, Nov. 2020.

[39] X. Gao *et al.*, "In situ strengthening of CrMnFeCoNi high-entropy alloy with Al realized by laser

additive manufacturing," *J. Alloys Compd.*, vol. 847, p. 156563, Dec. 2020.

[40] D. Yuan, S. Shao, C. Guo, F. Jiang, and J. Wang, "Grain refining of Ti-6Al-4V alloy fabricated by laser and wire additive manufacturing assisted with ultrasonic vibration," *Ultrason. Sonochem.*, vol. 73, p. 105472, May 2021.

[41] J. J. de Damborenea, M. A. Arenas, M. A. Larosa, A. L. Jardini, C. A. de Carvalho Zavaglia, and A. Conde, "Corrosion of Ti6Al4V pins produced by direct metal laser sintering," *Appl. Surf. Sci.*, vol. 393, pp. 340–347, Jan. 2017.

[42] O. S. Fatoba, A. M. Lasisi, O. M. Ikumapayi, S. A. Akinlabi, and E. T. Akinlabi, "Computational modelling of laser additive manufactured (LAM) Titanium alloy grade 5," *Mater. Today Proc.*, Dec. 2020.

[43] Y. Liu and Y. Zhang, "Microstructure and mechanical properties of TA15-Ti2AlNb bimetallic structures by laser additive manufacturing," *Mater. Sci. Eng. A*, vol. 795, p. 140019, Sep. 2020.

[44] Y. Li *et al.*, "Influence of environmental constraints and carrier gas velocity on powder concentration and temperature distribution during laser inside additive manufacturing process," *CIRP J. Manuf. Sci. Technol.*, vol. 32, pp. 70–80, Jan. 2021.

[45] C. Molina, A. Araujo, K. Bell, P. F. Mendez, and M. Chapetti, "Fatigue life of laser additive manufacturing repaired steel component," *Eng. Fract. Mech.*, vol. 241, p. 107417, Jan. 2021.

[46] V. I. Aladesanmi, O. S. Fatoba, E. T. Akinlabi, and O. M. Ikumapayi, "Analysis of wear properties and surface roughness of laser additive manufactured (LAM) Ti and TiB2 metal matrix composite," *Mater. Today Proc.*, Dec. 2020.

[47] Q. Liu *et al.*, "Microstructure and mechanical properties of LMD-SLM hybrid forming Ti6Al4V alloy," *Mater. Sci. Eng. A*, vol. 660, pp. 24–33, Apr. 2016.

[48] D. Chen, Y. Cai, Y. Luo, J. Tu, and F. Tang, "Analysis on the microstructure regulation based on the pulsed laser oscillating molten pool in Laser-PTA additive manufacturing," *J. Manuf. Process.*, vol. 59, pp. 587–594, Nov. 2020.

[49] V. I. Aladesanmi, O. S. Fatoba, E. T. Akinlabi, and O. M. Ikumapayi, "Regression analysis of hardness property of laser additive manufactured (LAM) Ti and TiB2 metal matrix composite," *Mater. Today Proc.*, Dec. 2020.

[50] ISO, "ISO - ISO 17296-2:2015 - Additive manufacturing — General principles — Part 2: Overview of process categories and feedstock." [Online]. Available: https://www.iso.org/standard/61626.html. [Accessed: 07-Feb-2021].

[51] I. L. de C. Camargo, M. M. Morais, C. A. Fortulan, and M. C. Branciforti, "A review on the rheological behavior and formulations of ceramic suspensions for vat photopolymerization," *Ceram. Int.*, Jan. 2021.

[52] R. V. Pazhamannil and P. Govindan, "Current state and future scope of additive manufacturing technologies via vat photopolymerization," *Mater. Today Proc.*, Jan. 2021.

[53] X. Xu, A. Awad, P. Robles-Martinez, S. Gaisford, A. Goyanes, and A. W. Basit, "Vat photopolymerization 3D printing for advanced drug delivery and medical device applications," *Journal of Controlled Release*. Elsevier B.V., 05-Oct-2020.

[54] K. Yuvaraj, A. Mohamed Ismail, P. Nagarajan, and S. Vigneshwaran, "Design and fabrication of gypsum prototypes based on binder jetting technology," *Mater. Today Proc.*, Jan. 2021.

[55] S. Manotham, S. Channasanon, P. Nanthananon, S. Tanodekaew, and P. Tesavibul, "Photosensitive binder jetting technique for the fabrication of alumina ceramic," *J. Manuf. Process.*, vol. 62, pp. 313–322, Feb. 2021.

[56] T. Q. Tran *et al.*, "3D printing of highly pure copper," *Metals (Basel).*, vol. 9, no. 7, pp. 12–20, 2019.

[57] J. Huebner, D. Kata, P. Rutkowski, P. Petrzak, and J. Kusiński, "Grain-boundary interaction between Inconel 625 and WC during laser metal deposition," *Materials (Basel).*, vol. 11, no. 10,

p. 1797, Sep. 2018.

[58] J. C. Najmon, S. Raeisi, and A. Tovar, "Review of additive manufacturing technologies and applications in the aerospace industry," in *Additive Manufacturing for the Aerospace Industry*, Elsevier, 2019, pp. 7–31.

[59] C. Culmone, G. Smit, and P. Breedveld, "Additive manufacturing of medical instruments: A state-of-the-art review," *Additive Manufacturing*, vol. 27. Elsevier B.V., pp. 461–473, May-2019.

[60] A. Maurel *et al.*, "Considering lithium-ion battery 3D-printing via thermoplastic material extrusion and polymer powder bed fusion," *Addit. Manuf.*, vol. 37, p. 101651, Jan. 2021.

[61] M. O. Shigueoka and N. Volpato, "Expanding manufacturing strategies to advance in porous media planning with material extrusion additive manufacturing," *Addit. Manuf.*, vol. 38, p. 101760, Feb. 2021.

[62] L. Li, R. McGuan, R. Isaac, P. Kavehpour, and R. Candler, "Improving precision of material extrusion 3D printing by in-situ monitoring & predicting 3D geometric deviation using conditional adversarial networks," *Addit. Manuf.*, vol. 38, p. 101695, Feb. 2021.

[63] A. Pugalendhi, R. Ranganathan, and S. Ganesan, "Impact of process parameters on mechanical behaviour in multi-material jetting," *Mater. Today Proc.*, Jan. 2020.

[64] E. Jabari, F. Liravi, E. Davoodi, L. Lin, and E. Toyserkani, "High speed 3D material-jetting additive manufacturing of viscous graphene-based ink with high electrical conductivity," *Addit. Manuf.*, vol. 35, p. 101330, Oct. 2020.

[65] T. Chen, J. Dilag, and S. Bateman, "Surface topology modification of organic substrates using material jetting technologies," *Mater. Des.*, vol. 196, p. 109116, Nov. 2020.

[66] Y. L. Tee, P. Tran, M. Leary, P. Pille, and M. Brandt, "3D Printing of polymer composites with material jetting: Mechanical and fractographic analysis," *Addit. Manuf.*, vol. 36, p. 101558, Dec. 2020.

[67] H. A. Derazkola, F. Khodabakhshi, and A. Simchi, "Evaluation of a polymer-steel laminated sheet composite structure produced by friction stir additive manufacturing (FSAM) technology," *Polym. Test.*, vol. 90, p. 106690, Oct. 2020.

[68] Q. Wu, M. Yao, M. Li, D. Cao, and B. Bai, "Nonlinear coupling vibrations of graphene composite laminated sheets impacted by particles," *Appl. Math. Model.*, vol. 93, pp. 75–88, May 2021.

[69] Y. Sun, P. Lin, and S. Yuan, "Deformation and fracture behavior of the novel NiAl alloy sheet with bimodal laminated structure by in-situ reaction synthesis," *Intermetallics*, vol. 127, p. 106944, Dec. 2020.

[70] H. Park, S. J. Kim, J. Lee, J. H. Kim, and D. Kim, "Delamination behavior analysis of steel/polymer/steel high-strength laminated sheets in a V-die bending test," *Int. J. Mech. Sci.*, vol. 173, p. 105430, May 2020.

[71] N. Nadammal *et al.*, "Critical role of scan strategies on the development of microstructure, texture, and residual stresses during laser powder bed fusion additive manufacturing," *Addit. Manuf.*, vol. 38, p. 101792, Feb. 2021.

[72] Y. Yang, F. van Keulen, and C. Ayas, "A computationally efficient thermal model for selective laser melting," *Addit. Manuf.*, vol. 31, no. July 2019, p. 100955, 2020.

[73] V. M. Rivas Santos, A. Thompson, D. Sims-Waterhouse, I. Maskery, P. Woolliams, and R. Leach, "Design and characterisation of an additive manufacturing benchmarking artefact following a design-for-metrology approach," *Addit. Manuf.*, vol. 32, no. November 2019, p. 100964, 2020.

[74] Q. Guo *et al.*, "In-situ full-field mapping of melt flow dynamics in laser metal additive manufacturing," *Addit. Manuf.*, vol. 31, no. November 2019, p. 100939, 2020.

[75] P. Mair *et al.*, “Laser powder bed fusion of nano-CaB6 decorated 2024 aluminum alloy,” *J. Alloys Compd.*, vol. 863, p. 158714, Jan. 2021.

[76] D. Dev Singh, T. Mahender, and A. Raji Reddy, “Powder bed fusion process: A brief review,” *Mater. Today Proc.*, Sep. 2020.

[77] I. I.-I. Geneva, T. Switzerland, and undefined 2016, “17296-2 Additive Manufacturing—General Principles—Part2: Overview of Process Categories and Feedstock.”

[78] G. K. Mishra, C. P. Paul, A. K. Rai, A. K. Agrawal, S. K. Rai, and K. S. Bindra, “Experimental investigation on Laser Directed Energy Deposition based additive manufacturing of Al2O3 bulk structures,” *Ceram. Int.*, vol. 47, no. 4, pp. 5708–5720, Feb. 2021.

[79] Y. Wu *et al.*, “Fabrication of TiAl alloy with no multiple heat-affected bands using continuous direct energy deposition,” *Mater. Lett.*, vol. 281, p. 128581, Dec. 2020.

[80] P. H. Smith, J. W. Murray, D. O. Jones, J. Segal, and A. T. Clare, “Magnetically assisted directed energy deposition,” *J. Mater. Process. Technol.*, vol. 288, p. 116892, Feb. 2021.

[81] J. P. Kelly, J. W. Elmer, F. J. Ryerson, J. R. I. Lee, and J. J. Haslam, “Directed energy deposition additive manufacturing of functionally graded Al-W composites,” *Addit. Manuf.*, vol. 39, p. 101845, Mar. 2021.

[82] A. I. Gorunov, “Additive manufacturing of Ti6Al4V parts using ultrasonic assisted direct energy deposition,” *J. Manuf. Process.*, vol. 59, pp. 545–556, Nov. 2020.

[83] Metal AM, “Design Advantages of Metal Additive Manufacturing.” [Online]. Available: https://www.metal-am.com/introduction-to-metal-additive-manufacturing-and-3d-printing/design-advantages-of-metal-additive-manufacturing/. [Accessed: 23-Jul-2020].

[84] K. Shah, A. J. Pinkerton, A. Salman, and L. Li, “Effects of melt pool variables and process parameters in laser direct metal deposition of aerospace alloys,” *Mater. Manuf. Process.*, vol. 25, no. 12, pp. 1372–1380, Dec. 2010.

[85] M. N. Ahsan, A. J. Pinkerton, R. J. Moat, and J. Shackleton, “A comparative study of laser direct metal deposition characteristics using gas and plasma-atomized Ti-6Al-4V powders,” *Mater. Sci. Eng. A*, vol. 528, no. 25–26, pp. 7648–7657, Sep. 2011.

[86] R. Brockmann, A. Candel-Ruiz, S. Kaufmann, and O. Müllerschön, “Strategies for high deposition rate additive manufacturing by laser metal deposition,” in *International Congress on Applications of Lasers & Electro-Optics*, 2018, vol. 2015, no. 1, pp. 680–683.

[87] D. Chioibasu *et al.*, “Prototype orthopedic bone plates 3D printed by laser melting deposition,” *Materials (Basel).*, vol. 16, no. 6, Mar. 2019.

[88] I. Ghiuta *et al.*, “The influence of powder particle and grain size on parts manufacturing by powder bed fusion,” *Mater. Sci. Forum*, vol. 941 MSF, pp. 1585–1590, 2018.

[89] S. Comsa, T. C. Milian, and D. Gheorghiu, “The influence of exposure parameters on the quality of the parts built by selective laser prototyping,” *Int. J. Mechatronics Appl. Mech.*, vol. 2017, no. 2, pp. 144–149, 2017.

[90] D. Besnea, D. Rizescu, and C. I. Rizescu, “Additive Technologies and Materials Used for Making,” *Int. J. Mechatronics Appl. Mech.*, no. 3, pp. 13–17, 2018.

[91] C. Moldovan, C. Cosma, P. Berce, and N. Balc, “Theoretical analysis and practical case studies of sla, polyjet and fdm manufacturing techniques,” *Acta Tech. Napocensis-Series Appl. Math. Mech. Eng.*, vol. 61, no. 3, pp. 369–378, 2018.

[92] T. Bedo *et al.*, “Method for translating 3D bone defects into personalized implants made by additive manufacturing,” in *Materials Today: Proceedings*, 2019, vol. 19, pp. 1032–1040.

[93] C. Cosma, N. Balc, P. Berce, A. Popan, A. Cosma, and A. Burde, “DIRECT MANUFACTURING OF CUSTOMIZED IMPLANTS FROM BIOMETALS, BY 3D PRINTING,” 2017.

[94] G. Armencea *et al.*, “Technical queries of a 3D design custom-made implant made from titanium

particles for maxillofacial bone reconstruction," *Part. Sci. Technol.*, vol. 38, no. 6, pp. 676–684, Mar. 2020.

[95] C. Cosma, J. Kessler, A. Gebhardt, I. Campbell, and N. Balc, "Improving the Mechanical Strength of Dental Applications and Lattice Structures SLM Processed," *Materials (Basel).*, vol. 13, no. 4, p. 905, Feb. 2020.

[96] M. A. Baciu, E. R. Baciu, C. Bejinariu, S. L. Toma, A. Danila, and C. Baciu, "Influence of Selective Laser Melting Processing Parameters of Co-Cr-W Powders on the Roughness of Exterior Surfaces," *IOP Conf. Ser. Mater. Sci. Eng.*, vol. 374, no. 1, 2018.

[97] "THE IMPORTANCE OF OPTIMIZATION OF LATTICE STRUCTURES FOR BIOMEDICAL APPLICATIONS - ProQuest." [Online]. Available: https://search.proquest.com/openview/a50d8f76ff44bda07c74d4d947dd5470/1?pq-origsite=gscholar&cbl=366251. [Accessed: 24-Jul-2020].

[98] G. Razvan Buican, G. Oancea, and R. F. Martins, "Study on SLM manufacturing of teeth used for dental tools testing," EDP Sciences, 2017.

[99] "Weight reduction by topology optimization of an engine subframe mount, designed for additive manufacturing production | Elsevier Enhanced Reader." [Online]. Available: https://reader.elsevier.com/reader/sd/pii/S2214785319329451?token=AE0450E6231BA290A9783C07B826A6BA9E4C1650994D859795CC18F9DD6AFEF58CC3F83AFAAA65D36C9F1BE4D7018C6C. [Accessed: 24-Jul-2020].

[100] Comoti, "Turbo Scientific Journal," 2019. [Online]. Available: http://www.comoti.ro/docs/jurnal/TURBO_Vol_VI_no.2_dec. 2019.pdf. [Accessed: 24-Jul-2020].

[101] I. Gheorghe, D. Ciobota, C. Stanca, A. Pacioga, D. Gheorghiu, and N. Tsohas, "New technologies for building complex parts from plastic powders on laser sintering systems," *Rom. Rev. Precis. Mech. Opt. Mechatronics*, vol. 2015, no. 48, pp. 213–218, 2015.

[102] G. Matache, M. Vladut, A. Paraschiv, and R. M. Condruz, "Edge and corner effects in selective laser melting of IN 625 alloy," *Manuf. Rev.*, vol. 7, p. 8, 2020.

[103] M. R. Condruz, G. Matache, A. Paraschiv, T. Badea, and V. Badilita, "High temperature oxidation behavior of selective laser melting manufactured in 625," *Metals (Basel).*, vol. 10, no. 5, 2020.

[104] C. Gabor, M. A. Pop, D. Magli, T. Bedo, S. I. Munteanu, and D. Munteanu, "The optimization of the production procedure in relation to the mechanical properties of additively manufactured parts," *Mater. Today Proc.*, vol. 19, pp. 1008–1013, Jan. 2019.

[105] D. Cristea, M. A. Pop, C. Faraian, and D. Munteanu, "The influence of additive manufacturing parameters on the structural and mechanical properties of acrylonitrile butadiene styrene (ABS) parts produced by fused filament fabrication," *IOP Conf. Ser. Mater. Sci. Eng.*, vol. 682, no. 1, 2019.

[106] I. A. H. Kursat Celik, Ozkan Kose, Mihaela-Elena Ulmeanu, Allan E.W. Rennie, Thomas N. Abram, "Design and Rapid Prototyping of a Medical Face Shield for Healthcare Workers Design and Additive Manufacturing of a Medical Face Shield for Healthcare Workers Battling Coronavirus ( COVID-19 )," *Int. J. Bioprinting*, no. July, 2020.

[107] "Cercetare si Dezvoltare | Compa." [Online]. Available: https://compa.ro/despre-compa/cercetare-si-dezvoltare. [Accessed: 17-Aug-2020].

[108] E. Rauch, M. Unterhofer, and P. Dallasega, "Industry sector analysis for the application of additive manufacturing in smart and distributed manufacturing systems," *Manuf. Lett.*, vol. 15, pp. 126–131, Jan. 2018.

[109] S. Singh and S. Ramakrishna, "Biomedical applications of additive manufacturing: Present and future," *Current Opinion in Biomedical Engineering*, vol. 2. Elsevier B.V., pp. 105–115, 01-Jun-2017.

[110] H. Fukuda, "Additive Manufacturing Technology for Orthopedic Implants," Springer, Berlin, Heidelberg, 2015, pp. 3–26.

[111] A. Emelogu, M. Marufuzzaman, S. M. Thompson, N. Shamsaei, and L. Bian, "Additive manufacturing of biomedical implants: A feasibility assessment via supply-chain cost analysis," *Addit. Manuf.*, vol. 11, pp. 97–113, Jul. 2016.

[112] M. A. Mahmood *et al.*, "Three-jet powder flow and laser–powder interaction in laser melting deposition: Modelling versus experimental correlations," *Metals (Basel).*, vol. 10, no. 9, pp. 1–17, 2020.

[113] A. J. Pinkerton and L. Li, "An analytical model of energy distribution in laser direct metal deposition," in *Proceedings of the Institution of Mechanical Engineers, Part B: Journal of Engineering Manufacture*, 2004, vol. 218, no. 4, pp. 363–374.

[114] M. N. Ahsan and A. J. Pinkerton, "An analytical–numerical model of laser direct metal deposition track and microstructure formation," *Model. Simul. Mater. Sci. Eng.*, vol. 19, no. 5, p. 055003, Jun. 2011.

[115] Z. Liu, H. C. Zhang, S. Peng, H. Kim, D. Du, and W. Cong, "Analytical modeling and experimental validation of powder stream distribution during direct energy deposition," *Addit. Manuf.*, vol. 30, p. 100848, Dec. 2019.

[116] S. Liu and Y. C. Shin, "Simulation and experimental studies on microstructure evolution of resolidified dendritic TiCx in laser direct deposited Ti-TiC composite," *Mater. Des.*, vol. 159, pp. 212–223, Dec. 2018.

[117] S. Liu and Y. C. Shin, "The influences of melting degree of TiC reinforcements on microstructure and mechanical properties of laser direct deposited Ti6Al4V-TiC composites," *Mater. Des.*, vol. 136, pp. 185–195, Dec. 2017.

[118] T. Petrat, B. Graf, A. Gumenyuk, and M. Rethmeier, "Laser metal deposition as repair technology for a gas turbine burner made of inconel 718," in *Physics Procedia*, 2016, vol. 83, pp. 761–768.

[119] L. J. Kumar and C. G. K. Nair, "Laser metal deposition repair applications for Inconel 718 alloy," in *Materials Today: Proceedings*, 2017, vol. 4, no. 10, pp. 11068–11077.

[120] D. Chioibasu *et al.*, "Prototype Orthopedic Bone Plates 3D Printed by Laser Melting Deposition," *Materials (Basel).*, vol. 12, no. 6, p. 906, 2019.

[121] D. Chioibasu *et al.*, "Use of X-ray Computed Tomography for Assessing Defects in Ti Grade 5 Parts Produced by Laser Melting Deposition," *Metals (Basel).*, vol. 10, no. 11, p. 1408, Oct. 2020.

[122] S. Liu and Y. C. Shin, "Additive manufacturing of Ti6Al4V alloy: A review," *Mater. Des.*, vol. 164, p. 107552, 2019.

[123] G. Kasperovich and J. Hausmann, "Improvement of fatigue resistance and ductility of TiAl6V4 processed by selective laser melting," *J. Mater. Process. Technol.*, vol. 220, pp. 202–214, Jun. 2015.

[124] F. M. Abdullah, S. Anwar, and A. Al-Ahmari, "Thermomechanical simulations of residual stresses and distortion in electron beam melting with experimental validation for ti-6al-4v," *Metals (Basel).*, vol. 10, no. 9, pp. 1–28, Aug. 2020.

[125] J. Wang, L. Li, C. Tan, H. Liu, and P. Lin, "Microstructure and tensile properties of TiCp/Ti6Al4V titanium matrix composites manufactured by laser melting deposition," *J. Mater. Process. Technol.*, vol. 252, pp. 524–536, 2018.

[126] L. Li, J. Wang, P. Lin, and H. Liu, "Microstructure and mechanical properties of functionally graded TiCp/Ti6Al4V composite fabricated by laser melting deposition," *Ceram. Int.*, vol. 43, no. 18, pp. 16638–16651, Dec. 2017.

[127] H. Paydas, A. Mertens, R. Carrus, J. Lecomte-Beckers, and J. Tchoufang Tchuindjang, "Laser cladding as repair technology for Ti-6Al-4V alloy: Influence of building strategy on

microstructure and hardness," *Mater. Des.*, vol. 85, pp. 497–510, Nov. 2015.

[128] N. M. Baloyi, A. P. I. Popoola, and S. L. Pityana, "Microstructure, hardness and corrosion properties of laser processed Ti6Al4V-based composites," *Trans. Nonferrous Met. Soc. China (English Ed.*, vol. 25, no. 9, pp. 2912–2923, Sep. 2015.

[129] R. Raju, M. Duraiselvam, V. Petley, S. Verma, and R. Rajendran, "Microstructural and mechanical characterization of Ti6Al4V refurbished parts obtained by laser metal deposition," *Mater. Sci. Eng. A*, vol. 643, pp. 64–71, Sep. 2015.

[130] S. L. Sing, J. An, W. Y. Yeong, and F. E. Wiria, "Laser and electron-beam powder-bed additive manufacturing of metallic implants: A review on processes, materials and designs," *Journal of Orthopaedic Research*, vol. 34, no. 3. John Wiley and Sons Inc., pp. 369–385, 01-Mar-2016.

[131] M. Fischer *et al.*, "Synthesis and characterization of Ti-27.5Nb alloy made by CLAD® additive manufacturing process for biomedical applications," *Mater. Sci. Eng. C*, vol. 75, pp. 341–348, Jun. 2017.

[132] A. S. Gnedenkov *et al.*, "Direct laser deposition as a method of biodegradable magnesium implant manufacturing," in *Journal of Physics: Conference Series*, 2018, vol. 1092, no. 1, p. 12044.

[133] M. N. Ahsan, C. P. Paul, L. M. Kukreja, and A. J. Pinkerton, "Porous structures fabrication by continuous and pulsed laser metal deposition for biomedical applications; Modelling and experimental investigation," *J. Mater. Process. Technol.*, vol. 211, no. 4, pp. 602–609, Apr. 2011.

[134] V. K. Balla, W. Xue, S. Bose, and A. Bandyopadhyay, "Laser-assisted Zr/ZrO2 coating on Ti for load-bearing implants," *Acta Biomater.*, vol. 5, no. 7, pp. 2800–2809, Sep. 2009.

[135] "Industrial 3D Printing for Medical Technology | EOS GmbH." [Online]. Available: https://www.eos.info/en/3d-printing-examples-applications/people-health/medical-3d-printing. [Accessed: 05-Jan-2021].

[136] J. Zhang, A. Q. Vo, X. Feng, S. Bandari, and M. A. Repka, "Pharmaceutical Additive Manufacturing: a Novel Tool for Complex and Personalized Drug Delivery Systems," *AAPS PharmSciTech*, vol. 19, no. 8. Springer New York LLC, pp. 3388–3402, 01-Nov-2018.

[137] L. Duta *et al.*, "In vivo assessment of bone enhancement in the case of 3d-printed implants functionalized with lithium-doped biological-derived hydroxyapatite coatings: A preliminary study on rabbits," *Coatings*, vol. 10, no. 10, pp. 1–21, Oct. 2020.

[138] L. Salou, A. Hoornaert, G. Louarn, and P. Layrolle, "Enhanced osseointegration of titanium implants with nanostructured surfaces: An experimental study in rabbits," *Acta Biomater.*, vol. 11, no. 1, pp. 494–502, Jan. 2015.

[139] R. Crespi, P. Capparé, G. E. Romanos, E. Mariani, E. Benasciutti, and E. Gherlone, "Corticocancellous porcine bone in the healing of human extraction sockets: combining histomorphometry with osteoblast gene expression profiles in vivo.," *Int. J. Oral Maxillofac. Implants*, vol. 26, no. 4, pp. 866–72, 2011.

[140] D. Chioibasu *et al.*, "Animal origin hydroxyapatite thin films synthesized by RF-Magnetron Sputtering on 3D printed cranial implants," *Metals (Basel).*, vol. 9, no. 12, pp. 1–24, 2019.

[141] A. C. Popescu *et al.*, "Biocompatible and bioactive nanostructured glass coatings synthesized by pulsed laser deposition: In vitro biological tests," *Appl. Surf. Sci.*, vol. 255, no. 10, pp. 5486–5490, Mar. 2009.